

1 **2005-2017 ozone trends and potential benefits of local measures as deduced from air quality measurements**  
2 **in the north of the Barcelona Metropolitan Area**

3 Jordi Massagué<sup>1, 2</sup>, Cristina Carnerero<sup>1, 2</sup>, Miguel Escudero<sup>3</sup>, José María Baldasano<sup>4</sup>, Andrés Alastuey<sup>1</sup>, Xavier  
4 Querol<sup>1</sup>

5 <sup>1</sup> Institute of Environmental Assessment and Water Research (IDAEA-CSIC), Barcelona, 08034, Spain.

6 <sup>2</sup> Department of Civil and Environmental Engineering, Universitat Politècnica de Catalunya, Barcelona, 08034, Spain.

7 <sup>3</sup> Centro Universitario de la Defensa, Academia General Militar, 50090 Zaragoza, Spain.

8 <sup>4</sup> Department of Projects and Construction Engineering (DEPC), Universitat Politècnica de Catalunya, 08028 Barcelona,  
9 Spain.

10 **Abstract**

11 We analyzed 2005–2017 data sets on ozone (O<sub>3</sub>) concentrations in an area (the Vic Plain) frequently affected  
12 by the atmospheric plume northward transport of Barcelona Metropolitan Area (BMA), the atmospheric basin  
13 of Spain recording the highest number of exceedances of the hourly O<sub>3</sub> information threshold (180 µg m<sup>-3</sup>).  
14 We aimed at evaluating the potential benefits of implementing local-BMA short-term measures to abate  
15 emissions of precursors. To this end, we analyzed in detail spatial and time variations of concentration of O<sub>3</sub>  
16 and nitrogen oxides (NO and NO<sub>2</sub>, including OMI remote sensing data for the latter). Subsequently, a sensitivity  
17 analysis is done with the air quality (AQ) data to evaluate potential O<sub>3</sub> reductions in the North of the BMA on  
18 Sundays, compared with weekdays as a consequence of the reduction in regional emissions of precursors.

19 The results showed a generalized decreasing trend for regional background O<sub>3</sub> as well as the well-known  
20 increase of urban O<sub>3</sub> and higher urban NO decreasing slopes compared with those of NO<sub>2</sub>. The most intensive  
21 O<sub>3</sub> episodes in the Vic Plain are caused by (i) a relatively high regional background O<sub>3</sub> (due to a mix of  
22 continental, hemispheric–tropospheric and stratospheric contributions); (ii) intensive surface fumigation from  
23 mid-troposphere high O<sub>3</sub> upper layers arising from the concatenation of the vertical recirculation of air masses,  
24 but also by (iii) an important O<sub>3</sub> contribution from the northward transport/channeling of the pollution plume  
25 from the BMA. The high relevance of the local-daily O<sub>3</sub> contribution during the most intense pollution episodes  
26 is clearly supported by the O<sub>3</sub> (surface concentration) and NO<sub>2</sub> (OMI data) data analysis.

27 A maximum decrease potential (by applying short-term measures to abate emissions of O<sub>3</sub> precursors) of 49  
28 µg O<sub>3</sub> m<sup>-3</sup> (32%) of the average diurnal concentrations was determined. Structurally implemented measures,  
29 instead of episodically, could result in important additional O<sub>3</sub> decreases because not only the local O<sub>3</sub> coming  
30 from the BMA plume would be reduced but also the recirculated O<sub>3</sub> and thus the intensity of O<sub>3</sub> fumigation in  
31 the Plain. Therefore, it is highly probable that both structural and episodic measures to abate NO<sub>x</sub> and volatile  
32 organic compounds (VOCs) emissions in the BMA would result in evident reductions of O<sub>3</sub> in the Vic Plain.

33 **Keywords:** tropospheric ozone, regional pollution, photochemistry, air quality trends.

34 **1. Introduction**

35 Tropospheric ozone (O<sub>3</sub>) is a secondary atmospheric pollutant produced by the photooxidation of volatile  
36 organic compounds (VOCs) in the presence of nitrogen oxides (NO<sub>x</sub> = NO + NO<sub>2</sub>). Its generation is enhanced  
37 under high temperature and solar radiation (Monks et al., 2015 and references therein). Thus, O<sub>3</sub> maxima  
38 occur generally in the afternoon, with the highest levels typically registered in summer, when exceedances of  
39 regulatory thresholds are most frequent.

40 O<sub>3</sub> is one of the key air pollutants affecting human health and the environment (WHO, 2006, 2013a, 2013b;  
41 GBD, 2016; Fowler et al., 2009; IPCC, 2013). According to EEA (2018), in the period 2013–2015, more than 95%  
42 of the urban population in the EU-28 was exposed to O<sub>3</sub> levels exceeding the WHO guidelines set for the  
43 protection of the human health (maximum daily 8-h average concentration of 100 µg m<sup>-3</sup>).

44 On a global scale, approximately 90% of the tropospheric O<sub>3</sub> is produced photochemically within the  
45 troposphere (Stevenson et al., 2006; Young et al., 2013), the remaining part being transported from the  
46 stratosphere (McLinden et al., 2000; Olson et al., 2001). The main global sink of tropospheric O<sub>3</sub> is photolysis  
47 in the presence of water vapor. Dry deposition, mainly by vegetation, is also an important sink in the  
48 continental planetary boundary layer (PBL) (Jacob and Winner, 2009).

49 On a regional scale, O<sub>3</sub> levels vary substantially depending on the different chemical environments within the  
50 troposphere. O<sub>3</sub> chemical destruction is largest where water vapor concentrations are high, mainly in the lower  
51 troposphere, and in polluted areas where there is direct O<sub>3</sub> destruction by titration. Thus, the hourly, daily and  
52 annual variations in O<sub>3</sub> levels at a given location are determined by several factors, including the geographical  
53 characteristics, the predominant meteorological conditions and the proximity to large sources of O<sub>3</sub> precursors  
54 (Logan, 1985).

55 Southern Europe, especially the Mediterranean basin, is the most exposed to O<sub>3</sub> pollution in Europe (EEA,  
56 2018) due to the specific prevailing meteorological conditions during warm seasons, regional pollutant  
57 emissions, high biogenic VOCs' (BVOCs) emissions in spring and summer and the vertical recirculation of air  
58 masses due to the particular orographic features that help stagnation–recirculation episodes (Millán et al.,  
59 2000; EC, 2002, 2004; Millán, 2009; Diéguez et al., 2009, 2014; Valverde et al., 2016). Periods with high O<sub>3</sub>  
60 concentrations often last for several days and can be detected simultaneously in several countries. Lelieveld  
61 et al. (2002) reported that during summer, O<sub>3</sub> concentrations are 2.5–3 times higher than in the hemispheric  
62 background troposphere. High O<sub>3</sub> levels are common in the area, not only at the surface but also throughout  
63 the PBL (Millán et al., 1997; Gangoiiti et al., 2001; Kalabokas et al., 2007). Photochemical O<sub>3</sub> production is  
64 favored due to frequent anticyclonic conditions with clear skies during summer, causing high insolation and  
65 temperatures and low rainfall. Besides, the emissions from the sources located around the basin, which is  
66 highly populated and industrialized, and the long-range transport of O<sub>3</sub> contribute to the high concentrations  
67 (Millán et al., 2000; Lelieveld et al., 2002; Gerasopoulos, 2005; Safieddine et al., 2014).

68 In this context, the design of efficient O<sub>3</sub> abatement policies is difficult due to the following circumstances:

- 69 • The meteorology driving O<sub>3</sub> dynamics is highly influenced by the complex topography surrounding the  
70 basin (see the above references for vertical recirculation of air masses and Mantilla et al., 1997;  
71 Salvador et al., 1997; Jiménez and Baldasano, 2004; Stein et al., 2004).
- 72 • The complex nonlinear chemical reactions between NO<sub>x</sub> and VOCs (Finlayson-Pitts and Pitts, 1993;  
73 Pusede et al., 2015), in addition to the vast variety of the VOCs precursors involved and the  
74 involvement of BVOCs in O<sub>3</sub> formation and destruction (Hewitt et al., 2011).
- 75 • The transboundary transport of air masses containing significant concentrations of O<sub>3</sub> and its  
76 precursors, which contribute to increased O<sub>3</sub> levels, mainly background concentrations (UNECE, 2010).
- 77 • The contribution from stratospheric intrusions (Kalabokas et al., 2007).
- 78 • The fact that O<sub>3</sub> concentrations tend to be higher in rural areas (EEA, 2018), where local mitigation  
79 plans are frequently inefficient, because the emission of precursors takes place mostly in distant urban  
80 and industrial agglomerations.

81  
82 Sicard et al. (2013) analyzed O<sub>3</sub> time trends during 2000–2010 in the Mediterranean and observed a slight  
83 decrease of annual O<sub>3</sub> averages (–0.4% per year) at rural sites, and an increase at urban and suburban stations  
84 (+0.6% and +0.4%, respectively). They attributed the reduction at rural sites to the abatement of NO<sub>x</sub> and VOCs  
85 emissions in the EU. Paradoxically, this led to an increase in O<sub>3</sub> at urban sites due to a reduction in the titration  
86 by NO. Their results also suggested a tendency to converge at remote and urban sites. Paoletti et al. (2014)  
87 also reported convergence in the EU and the US in the period 1990–2010 but found increasing annual averages  
88 at both rural and urban sites, with a faster increase in urban areas. Querol et al. (2016) determined that O<sub>3</sub>  
89 levels in Spain remained constant at rural sites and increased at urban sites in the period 2000–2015. This was  
90 suggested to be a result of the preferential reduction of NO versus NO<sub>2</sub>, supported by the lack of a clear trend  
91 in O<sub>x</sub> (O<sub>3</sub> + NO<sub>2</sub>). They also found that the target value was constantly exceeded in large areas of the Spanish  
92 territory, while most of the exceedances of the information threshold took place in July, mainly downwind of

93 urban areas and industrial sites, and were highly influenced by summer heatwaves. The Vic Plain (located  
94 north of Barcelona) was the area registering the most annual exceedances of the information threshold in  
95 Spain, with an average of 15 exceedances per year per site.

96 In this study, we analyze NO, NO<sub>2</sub> and O<sub>3</sub> surface data around the Barcelona Metropolitan Area (BMA) and the  
97 Vic Plain, as well as NO<sub>2</sub> satellite observations, in the period 2005–2017, with the aim of better understanding  
98 the occurrence of high O<sub>3</sub> episodes in the area on a long-term basis. Previous studies in this region focused on  
99 specific episodes, whereas we aim at assessing the spatial distribution, time trends and temporal patterns of  
100 O<sub>3</sub> and its precursors, and the exceedances of the information threshold on a long time series. After better  
101 understanding the 2005–2017 O<sub>3</sub> episodes, we aim to evaluate, as a first approximation using air quality  
102 monitoring and OMI remote sensing data, the effect that episodic mitigation measures of O<sub>3</sub> precursors would  
103 have in the O<sub>x</sub> concentrations in the Vic Plain.

104 We recognize that the O<sub>3</sub> problem has to be studied with executable models with dispersion and  
105 photochemical modules, which allow performing sensitivity analyses. It is also well recognized that there is a  
106 complex O<sub>3</sub> phenomenology in the study area and that although models have greatly improved in the last 10  
107 years, there are still problems in reproducing some of the processes in detail, such as the channeling of O<sub>3</sub>  
108 plumes in narrow valleys or the vertical recirculation patterns. Our study intends to obtain a sensitivity analysis  
109 for O<sub>3</sub> concentrations using air quality data. Ongoing collaboration is being established with modelers to try to  
110 validate model outputs with this experimental sensitivity analysis and then to implement a prediction system  
111 for abating efficiently O<sub>3</sub> precursors to reduce O<sub>3</sub> concentrations, for which executable models are the solely  
112 tool available.

## 113 **2. Methodology**

114

### 115 **2.1. The area of study**

116 The study is set in central Catalonia (Spain), in the north-eastern corner of the Iberian Peninsula (Figure 1).  
117 Characterized by a Mediterranean climate, summers are hot and dry with clear skies. In the 21<sup>st</sup> century, heat  
118 waves have occurred frequently in the area, often associated with high O<sub>3</sub> levels (Vautard et al., 2007; Guerova  
119 et al., 2007; Querol et al., 2016; Guo et al., 2017).

120 The capital city, Barcelona, is located on the shoreline of the Mediterranean Sea. Two sets of mountain chains  
121 lie parallel to the coastline (SW–NE orientation) and enclose the Pre-coastal Depression: the Coastal (250–500  
122 m above sea level (a.s.l.)) and the Pre-Coastal (1000–1500 m a.s.l.) mountain ranges. The Vic Plain, situated  
123 45–70 km North of Barcelona (500 m a.s.l.) is a 230 km<sup>2</sup> plateau that stretches along a S–N direction and is  
124 surrounded by high mountains (over 1000 m a.s.l.). The complex topography of the area protects it from  
125 Atlantic advections and continental air masses but also hinders the dispersion of pollutants (Balasano et al.,  
126 1994). The two main rivers in the area (Llobregat and Besòs) flow perpendicularly to the sea and frame the  
127 city of Barcelona. Both rivers' valleys play an important role in the creation of air-flow patterns. The Congost  
128 River is a tributary to the Besòs River and its valley connects the Vic Plain with the Pre-coastal Depression.

129 The BMA stretches across the Pre-Coastal and Coastal Depressions and is a densely populated (>1500 people  
130 per km<sup>2</sup>, MFom, 2017) and highly industrialized area with large emissions originating from road traffic, aircraft,  
131 shipping, industries, biomass burning, power generation and livestock.

132 During summer, the coupling of daily upslope winds and sea breezes may cause the penetration of polluted  
133 air masses up to 160 km inland, channeled from the BMA northward by the complex orography of the area.  
134 These air masses are injected at high altitudes (2000–3000 m a.s.l.) by the Pyrenean mountain ranges. At night  
135 time, the land breeze prevails, and winds flow toward the sea followed by subsidence sinking of the air mass,  
136 which can be transported again by the sea breeze of the following day (Millán et al., 1997, 2000, 2002; Toll  
137 and Balasano, 2000; Gangoiti, 2001; Gonçalves et al., 2009; Millán, 2014; Valverde et al., 2016). Under  
138 conditions of a lack of large-scale forcing and the development of a thermal low over the Iberian Peninsula  
139 that forces the confluence of surface winds from coastal areas toward the central plateau, this vertical  
140 recirculation of the air masses results in regional summer O<sub>3</sub> episodes in the Western Mediterranean. In

141 addition, there might be external O<sub>3</sub> contributions, such as hemispheric transport or stratospheric intrusions  
142 (Kalabokas et al., 2007, 2008, 2017; Querol et al., 2017, 2018).

## 143 **2.2. Air quality, meteorological and remote sensing data**

144 We evaluated O<sub>3</sub> and NO<sub>x</sub> AQ data together with meteorological variables and satellite observations of  
145 background NO<sub>2</sub>.

146 The regional government of Catalonia (Generalitat de Catalunya, GC) has a monitoring network of stations  
147 that provides average hourly data of air pollutants (XVPCA, GC, 2017a, b). We selected a total of 25 stations  
148 (see Figure 2). To study the O<sub>3</sub> phenomenology in the Vic Plain, we selected the 8 stations marked in green,  
149 which met the following constraints: (i) location along the S–N axis (Barcelona–Vic Plain–Pre-Pyrenean Range);  
150 (ii) availability of O<sub>3</sub> measurements; (iii) availability of at least 9 years of data in the period 2005–2017, with at  
151 least 75% data coverage from April to September. The remaining selected stations (used only as reference  
152 ones for interpreting data from the main Vic-BMA axis stations) met the following criteria: (i) location across  
153 the Catalan territory, and (ii) availability of a minimum of 5 years of valid O<sub>3</sub> data in the period 2005–2017. We  
154 chose this period due to the poor data coverage of most of the AQ sites in the regional network of AQ  
155 monitoring stations before 2005.

156 In addition, we selected wind and temperature data from 5 meteorological stations from the Network of  
157 Automatic Meteorological Stations (XEMA, Meteocat, 2017) closely located to the previously selected AQ  
158 stations, as well as solar radiation data from two solar radiation sites from the Catalan Network of Solar  
159 Radiation Measurement Stations (ICAEN-UPC, 2018) located in the cities of Girona and Barcelona.

160 We also used daily tropospheric NO<sub>2</sub> column satellite measurements using the Ozone Monitoring Instrument  
161 (OMI) spectrometer aboard NASA's Earth Observing System (EOS) Aura satellite (see OMI, 2012; Krotkov and  
162 Veefkind, 2016). The measurements are suitable for all atmospheric conditions and for sky conditions where  
163 cloud fraction is less than 30% binned and averaged into 0.25° × 0.25° global grids.

## 164 **2.3. Data analysis**

### 165 **2.3.1. O<sub>x</sub> calculations**

166 We calculated O<sub>x</sub> concentrations to better interpret O<sub>3</sub> dynamics. Kley and Gleiss (1994) proposed the concept  
167 of O<sub>x</sub> to improve the spatial and temporal variability analysis by decreasing the effect of titration of O<sub>3</sub> by NO  
168 with the subsequent consumption of O<sub>3</sub> in areas where NO concentrations are high. Concentrations were  
169 transformed to ppb units using the conversion factors at 20 °C and 1 atm (DEFRA, 2014).

170 O<sub>x</sub> concentrations were only calculated if there were at least 6 simultaneous hourly recordings of O<sub>3</sub> and NO<sub>2</sub>  
171 from 12:00 to 19:00 h, June–August, in the period 2005–2017. The stations used for these calculations were  
172 those located along the S–N axis (Barcelona–Vic Plain–Pre-Pyrenean Range).

### 173 **2.3.2. Variability of concentrations across the air quality monitoring network**

174 To study the variability of concentrations of NO, NO<sub>2</sub>, O<sub>3</sub> and O<sub>x</sub> across the air quality monitoring network we  
175 calculated June–August averages (months recording the highest concentrations of O<sub>3</sub> in the area) from hourly  
176 concentrations provided by all the selected AQ sites. For each of them, we calculated daily averages and  
177 daytime high averages (12:00 to 19:00 h).

### 178 **2.3.3. Time trends**

180 By means of the Mann–Kendall method, we analyzed time trends for NO, NO<sub>2</sub> and O<sub>3</sub> for the period 2005–  
181 2017. In addition, we used the Theil–Sen statistical estimator (Theil, 1950; Sen, 1968) implemented in the R  
182 package Openair (Carslaw and Ropkins, 2012) to obtain the regression parameters of the trends (slope,  
183 uncertainty and p-value) estimated via bootstrap resampling. We examined the annual time trends of seasonal  
184 averages (April–September) for each pollutant. Data used for these calculations were selected according to  
185 the recommendations in EMEP-CCC (2016): the stations considered have at least 10 years of data (75% of the  
186 total period considered, 2005–2017) and at least 75% of the data is available within each season. In addition,

187 we analyzed annual time trends of tropospheric NO<sub>2</sub> measured by satellite along the S–N axis and of  
188 greenhouse gases (GHGs) emitted in Catalonia and the average number of vehicles entering the city of  
189 Barcelona.

#### 190 **2.3.4. Assessment of O<sub>3</sub> objectives according to air quality standards**

191 We identified the maximum daily 8-hour average concentrations by examining 8-h running averages using  
192 hourly data in the period 2005–2017. Each 8-h average was assigned to the day on which it ended (i.e., the  
193 first average of one day starts at 17:00 h on the previous day), as determined by EC (2008).

194 To assess the time trends and patterns of the Exceedances of Hourly Information Thresholds (EHITs)  
195 established by EC (2008) (hourly mean of O<sub>3</sub> concentration greater than 180 µg m<sup>-3</sup>), we used all the data,  
196 independently of the percentage of data availability.

#### 197 **2.3.5. Tropospheric NO<sub>2</sub> column**

198 We analyzed daily average Tropospheric Column NO<sub>2</sub> measurements from 2005 to 2017 aiming at two  
199 different goals. On the one hand, to quantify the tropospheric NO<sub>2</sub> in the area along the S–N axis and obtain  
200 annual time trends and monthly/weekly patterns. On the other hand, to assess qualitatively the tropospheric  
201 NO<sub>2</sub> across a regional scale (Western Mediterranean Europe) in two different scenarios, by means of visually  
202 finding patterns that might provide a better understanding of O<sub>3</sub> dynamics in our area of study. The scenarios  
203 were: days with the maximum 8-h O<sub>3</sub> average above the 75th percentile at the Vic Plain stations, and days  
204 with the maximum below the 25th percentile. See selected regions for retrieval of NO<sub>2</sub> satellite measurements  
205 in Figure S1.

#### 206 **2.3.6. Time conventions**

207 When expressing average concentrations, the times shown indicate the start time of the average. For example,  
208 12:00–19:00 h averages take into account data registered from 12:00 h to 19:59 h. All times are expressed as  
209 local time (UTC + 1 hour during winter and UTC + 2 hours during summer) and the 24-hour time clock  
210 convention is used.

### 211 **3. Results and discussion**

212

#### 213 **3.1. Variability of concentration of pollutants across the air quality monitoring network**

214 We analyzed the mean NO, NO<sub>2</sub>, O<sub>3</sub> and O<sub>x</sub> concentrations (June to August) in the study area in the period  
215 2005–2017.

216 As expected, the highest NO and NO<sub>2</sub> concentrations are registered in urban/suburban (U/SU) traffic sites in  
217 and around Barcelona (MON, GRA, MNR and CTL, 7–10 µg NO m<sup>-3</sup> and CTL and MON 30–36 µg NO<sub>2</sub> m<sup>-3</sup>). Also,  
218 as expected, the remote high-altitude rural background (RB) sites (MSY and MSC) register the lowest NO (<1  
219 µg m<sup>-3</sup>) and NO<sub>2</sub> (2–4 µg m<sup>-3</sup>) concentrations, see Figure S2.

220 The lowest June–August average O<sub>3</sub> concentrations (45–60 µg m<sup>-3</sup>) are recorded in the same U/SU traffic sites  
221 (MON, GRA, MNR and CTL) where titration by NO is notable, while the highest ones (>85 µg m<sup>-3</sup>) are recorded  
222 at the RB sites, MSC being the station recording the highest June–August O<sub>3</sub> levels (102 µg m<sup>-3</sup>). These spatial  
223 patterns are significantly different when we consider the 8-h daily averages of O<sub>3</sub> concentrations for June–  
224 August 12:00–19:00 h (Figure 3a). Thus, these concentrations are repeatedly high (85–115 µg m<sup>-3</sup>) in the whole  
225 area of study. The highest O<sub>3</sub> concentrations (>107 µg m<sup>-3</sup>) were recorded at the four sites located downwind  
226 of BMA along the S–N corridor (MSY, TON, VIC and MAN), and downwind of Tarragona (PON, RB station).  
227 Figure 3a also shows a positive O<sub>3</sub> gradient along the S–N axis (O<sub>3</sub> levels increase farther north) following the  
228 BMA plume transport and probably an increase of the mixing layer height (MLH). The higher O<sub>3</sub> production  
229 and/or fumigation in the northern areas are further supported by the parallel northward increasing O<sub>x</sub> gradient  
230 (δO<sub>x</sub> Figure 3b). Time series show that in 85% of the valid data in June–August (849 out of 1001 days in 2005–  
231 2017) this positive gradient is evident between CTL and TON (δO<sub>x,TON-CTL</sub> > 0). The average O<sub>x</sub> increase between

232 CTL in Barcelona and TON is 15 ppb. Taking into account the low NO<sub>2</sub> concentrations registered at this station,  
233 this is equivalent to approximately 29 µg m<sup>-3</sup> of O<sub>3</sub> (+30% O<sub>x</sub> in TON compared with CTL).

234 Thus, TON at the Vic Plain records the highest 12:00–19:00 h, June–August O<sub>x</sub> and O<sub>3</sub> concentrations in the  
235 study area. The MNR site also exhibits very high O<sub>x</sub> levels (Figure 3b) but these are mainly caused by primary  
236 NO<sub>2</sub> associated with traffic emissions.

## 237 3.2. Time patterns

### 238 3.2.1. Annual trends

240 Figure 4 shows the results of the trend analysis of NO, NO<sub>2</sub>, O<sub>3</sub> and O<sub>x</sub> averages (April to September, the O<sub>3</sub>  
241 season according to the European AQ Directive) by means of the Mann–Kendall test.

242 NO<sub>x</sub> levels exhibit a generalized and progressive decrease during the time period across Catalonia. In  
243 particular, NO<sub>2</sub> tended to decrease along the S–N axis during the period (U/SU sites CTL, MON and MAN  
244 registered –1.6, –2.0 and –1.3% year<sup>-1</sup>, respectively, with statistical significance in all cases). A similar trend  
245 was found for NO in these stations, with higher negative slopes (–2.2, –4.3 and –1.1% year<sup>-1</sup>, the latter without  
246 statistical significance).

247 The annual averages of tropospheric NO<sub>2</sub> across the S–N axis decreased by 35% from 2005 to 2017 (–3.4%  
248 year<sup>-1</sup> with statistical significance). The marked drop of NO<sub>2</sub> from 2007–2008 can be attributed to the  
249 reduction of emissions associated with the financial crisis starting in 2008. The time trends of average traffic  
250 (number of vehicles) entering Barcelona City on working days from 2005 to 2016 (Ajuntament de Barcelona,  
251 2010, 2017) and the GHGs emitted in Catalonia attributed to industry and power generation sectors calculated  
252 from the Emissions Inventories published by the Regional Government of Catalonia from 2005 to 2016 (GC,  
253 2017c) (Figure 5a) support this hypothesis. We found both decreasing trends to be statistically significant but  
254 the GHG emissions decreasing trend is significantly higher (–3.8% year<sup>-1</sup>) than the traffic (–1.2% year<sup>-1</sup>), which  
255 suggests that the crisis had a more severe effect on industry and power generation than on road traffic. This  
256 is also supported by a larger decrease of GHG emissions and OMI-NO<sub>2</sub> from 2005–2007 (precrisis) to 2008  
257 (start of the crisis) than BMA traffic counting and urban NO<sub>x</sub> levels (without a 2007–2008 steep change and a  
258 more progressive decrease, Figure 5b). Thus, in the BMA, the financial crisis caused a more progressive  
259 decrease (without a 2007–2008 steep change) of the circulating vehicles and therefore its associated  
260 emissions.

261 April–September O<sub>3</sub> and O<sub>x</sub> mean concentration trends are shown in Figure 4. The data show that seven out  
262 of the eight RB sites registered slight decreases in O<sub>3</sub> concentrations during the period (BdC, AGU and STP; –  
263 1.6% year<sup>-1</sup>, –1.1% year<sup>-1</sup> and –1.4% year<sup>-1</sup>, respectively, in all cases with statistical significance) while in BEG,  
264 PON, LSE and GAN the trends were not significant (not shown). As in several regions of Spain and Europe  
265 (Sicard et al., 2013; Paoletti et al., 2014; EEA, 2016; Querol et al., 2016; EMEP, 2016), the opposite trends are  
266 found for U/SU sites, with increases in O<sub>3</sub> concentrations during the period at some stations (CTL, MON, MAN,  
267 MAT, MNR and ALC; +0.4 to +3.2% year<sup>-1</sup> all with statistical significance). When considering O<sub>x</sub>, the increasing  
268 trends in U/SU sites are neutralized in some cases (CTL, MON, MAN, MAT and ALC). This, and the higher NO  
269 decreasing slopes compared with those of NO<sub>2</sub>, support the hypothesis that the U/SU O<sub>3</sub> increasing trends are  
270 probably caused by less O<sub>3</sub> titration (due to decrements in NO levels) instead of a higher O<sub>3</sub> generation. The  
271 marked decrease of the vehicle diesel emissions of NO/NO<sub>2</sub> time trends (Carslaw et al., 2016) might have  
272 caused this differential NO and NO<sub>2</sub> trends, although other causes cannot be discarded.

### 273 3.2.2. Monthly and daily patterns

274 Figure 6a shows 2005–2017 monthly average hourly O<sub>3</sub> concentrations measured at sites along the S–N axis,  
275 showing the occurrence of chronic-type episodes with repeated high O<sub>3</sub> concentrations (90–135 µg m<sup>-3</sup>) in the  
276 afternoon of April–September days at the Vic Plain sites (TON, VIC, MAN) and the remote RB sites (MSY and  
277 PAR).

278 Typically, at the remote RB stations, O<sub>3</sub> concentrations are high during the whole day throughout the year,  
279 and daily O<sub>3</sub> variations are narrower than at the other stations, with high average levels even during October–  
280 February (MSY: 50–70 and PAR: 50–80 µg m<sup>-3</sup>). During the night these mountain sites are less affected by NO  
281 titration, leading to high daily O<sub>3</sub> average concentrations. However, in summer, midday–afternoon  
282 concentrations are relatively lower than at the stations located in the S–N valley (TON, VIC, MAN).

283 Regarding monthly average daily O<sub>x</sub> (Figure 6b), the profiles of RB sites TON and MSY are very similar to the  
284 respective O<sub>3</sub> profiles. In the case of the BMA U/SU sites (CTL, MON, GRA), the nocturnal O<sub>x</sub> concentrations  
285 increase with respect to O<sub>3</sub> due to the addition of secondary NO<sub>2</sub> from titration. Midday–afternoon O<sub>x</sub> levels  
286 are much lower at the BMA U/SU stations than those in the S–N valley (MAN, TON), similarly to O<sub>3</sub> levels,  
287 supporting the contribution of local-regional O<sub>3</sub> from the BMA plume and/or from the fumigation of high-  
288 altitude reserve strata as MLH grows (Millán et al., 1997, 2000; Gangoi et al., 2001; Querol et al., 2017) as  
289 well as production of new O<sub>3</sub>.

### 290 **3.2.3. Weekly patterns**

291 Accordingly, Figure 7 shows the O<sub>3</sub> weekly patterns for these O<sub>3</sub> average concentrations. As expected, the  
292 variation of intra-annual concentration values is pronounced in the Vic Plain sites (TON, VIC, MAN; 20–45 µg  
293 m<sup>-3</sup> in December–January versus 110–125 µg m<sup>-3</sup> in July), due to the higher summer photochemistry, the more  
294 frequent summer BMA plume transport (due to intense sea breezing) and fumigation from upper atmospheric  
295 reservoirs across the S–N axis, and of the high O<sub>3</sub> titration in the populated valleys in winter. However, at the  
296 remote mountain sites of MSY and PAR, the intra-annual variability is much reduced (70–80 µg m<sup>-3</sup> in  
297 December versus 100–120 µg m<sup>-3</sup> in July) probably due to the reduced effect of NO titration at these higher  
298 altitude sites, and the influence of high-altitude O<sub>3</sub> regional reservoirs.

299 During the year, CTL, MON and GRA (U/SU sites around BMA) register very similar weekly patterns of the 8-h  
300 maxima, with a marked and typical high O<sub>3</sub> weekend effect, i.e., higher O<sub>3</sub> levels than during the week due to  
301 lower NO concentrations. From April to September, CTL O<sub>3</sub> 8-h concentrations are lower than MON's and  
302 GRA's (the latter located north of BMA following the sea breeze air mass transport), despite being very similar  
303 from October to March (when sea breezes are weaker). An O<sub>3</sub> weekend effect is also clearly evident during  
304 the winter months in the Vic Plain sites (TON, VIC, MAN) and MSY. However, from June to August, a marked  
305 inverse weekend effect is clearly evident at these same sites, with higher O<sub>3</sub> levels during weekdays. This  
306 points again to the clear influence of the emission of precursors from the BMA on the O<sub>3</sub> concentrations  
307 recorded at these inland sites.

308 We carried out a trend analysis of NO, NO<sub>2</sub> and O<sub>3</sub> levels measured at AQ sites and background NO<sub>2</sub> from  
309 remote sensing (OMI) for weekday (W) and weekend (WE) days independently. To this end we averaged the  
310 concentrations for 3 sites in the BMA (CTL, MON and GRA) and 3 receptor sites at the Vic Plain (TON, VIC and  
311 MAN), and considering WE to be Saturday, Sunday and Monday for the Vic AQ sites data (adding Mondays to  
312 account for the “clean Sunday effect”) and Saturday and Sunday for the BMA sites data.

313  
314 We estimated time trends of W and WE concentrations separately by the Mann-Kendall method along the  
315 study period. For O<sub>3</sub> (12:00 to 19:00 h) we found statistically significant increases in both the BMA and the Vic  
316 Plain. Increases of O<sub>3</sub> in the BMA double the ones in the Vic Plain and trends of W and WE are very similar per  
317 area (O<sub>3</sub> BMA W: +2.0 % year<sup>-1</sup>, O<sub>3</sub> BMA WE: +2.2 % year<sup>-1</sup>, O<sub>3</sub> Vic Plain W: +0.8 % year<sup>-1</sup>, O<sub>3</sub> Vic Plain WE: +1.0  
318 % year<sup>-1</sup>). As seen before, both NO and NO<sub>2</sub> levels (daily averages) in the BMA decrease in a statistically  
319 significant way, where NO decrements are larger than NO<sub>2</sub>. We found that the decrease of W NO levels is  
320 higher than the WE ones (NO BMA W: -3.4 % year<sup>-1</sup>, NO BMA WE: -2.7 % year<sup>-1</sup>) because emissions are higher  
321 during W days and these decreased along the period. Regarding NO<sub>2</sub>, W and WE decreases remain similar (NO<sub>2</sub>  
322 BMA W: -1.9 % year<sup>-1</sup>, NO<sub>2</sub> BMA WE: -1.7 % year<sup>-1</sup>) but lower than NO in both cases thus reducing the O<sub>3</sub>  
323 titration effects and increasing O<sub>3</sub> levels both in WE and W days. Regarding NO<sub>2</sub>-OMI levels, only W levels show  
324 a statistically significant decreasing trend (-3.4 % year<sup>-1</sup>) and not the WE levels.

325

326 We then assessed the variations of WE concentrations with respect to W's per year and plotted them by short  
327 tilted lines in Figure 8, where the left and right side of each tilted line represent W and WE concentrations  
328 respectively. These W to WE variations are then plotted in percentage by continuous lines (>0 depicts increase  
329 and <0 decrease W to WE). The upper plot shows O<sub>3</sub> data averaged from 12:00 to 19:00 h from the BMA and  
330 the Vic Plain, the middle plot daily averages of NO and NO<sub>2</sub> concentrations in BMA and the bottom plot, daily  
331 NO<sub>2</sub>-OMI levels along the S-N axis. The results evidence again a constant drop in W to WE NO<sub>x</sub> levels in the  
332 BMA along the period (negative percentages in the middle plot), with the subsequent O<sub>3</sub> weekend effect in  
333 the BMA (positive percentages in the upper plot). In the Vic Plain sites, O<sub>3</sub> concentrations remain constantly  
334 high along the study period showing inverse weekend effect almost during the whole period (negative  
335 percentages in the plot, except for 2005 to 2007 and 2017). Using the Mann-Kendall test to estimate trends  
336 for the W to WE variations we found a clear statistically significant decreasing trend along the period  
337 (reduction of the difference between W to WE levels: from -38% in 2005 to -17% in 2017, Figure 8 bottom).  
338 We attribute this to the decrease of W-NO<sub>x</sub> levels, described before for the annual averages.  
339

340 Furthermore we found a pattern of nearly parallel O<sub>3</sub> W to WE variation cycles between the Vic Plain and the  
341 BMA sites (Figure 8, upper). Due to the inverse W to WE O<sub>3</sub> at Vic and BMA, this parallel trend means in fact  
342 that maximum W to WE variations in the Vic Plain and the BMA tend to follow a reverse behavior, i.e.  
343 maximum W to WE variations in the BMA tend to occur when W to WE variations in the Vic Plain are minimum  
344 (for example 2007, 2010, 2014). NO<sub>x</sub> W to WE variations tend to follow a similar behavior than O<sub>3</sub> W to WE  
345 variations in the Vic Plain sites (mostly from 2008 to 2016) where years with high W to WE variations of NO<sub>x</sub>  
346 in the BMA tend to correspond to years with maximum O<sub>3</sub> W to WE variations in the Vic Plain (2009 and 2015).  
347 This behavior is probably associated to differences on air mass circulation patterns along the period (such as  
348 higher or lower breeze development). Those years with lower breeze development, the transport of the BMA  
349 plume is weaker; then NO<sub>x</sub> would tend to accumulate at the BMA (low W to WE NO<sub>x</sub> variation) which would  
350 generate more O<sub>3</sub> thus W to WE variation would be higher in the BMA and lower in the Vic Plain. As opposed,  
351 years with stronger breeze development and thus increased transport of the BMA plume, W to WE variations  
352 of NO<sub>x</sub> in the BMA are higher, W to WE variations of O<sub>3</sub> in the BMA are lower (less O<sub>3</sub> is generated during WE)  
353 and higher W to WE O<sub>3</sub> variations are recorded in the Vic Plain sites.  
354

### 355 **3.3. Peak O<sub>3</sub> concentrations patterns along the S–N axis**

356 July is the month of the year when most of the annual exceedances of the O<sub>3</sub> EHITs are recorded in Spain  
357 (Querol et al., 2016), including our area of study. Figure 9 shows the average O<sub>3</sub> and O<sub>x</sub> July hourly  
358 concentrations along the S–N axis during 2005–2017. A progressive time-shift and a marked positive  
359 northward gradient of O<sub>3</sub> and O<sub>x</sub> maxima are shown, pointing again to the gradual increase of O<sub>3</sub> and O<sub>x</sub> due  
360 to the plume transport, new O<sub>3</sub> formation and fumigation from upper reservoirs as MLH grows.

361 Figure 10a shows the 2005–2017 trends of the EHITs from the European AQ Directive (>180 µg m<sup>-3</sup> h<sup>-1</sup> mean;  
362 EC, 2008) registered at the selected sites in the S–N valley, as well as the average temperatures measured  
363 during July at early afternoon near Vic (at Gurb meteorological site), the background NO<sub>2</sub> measured by OMI  
364 (June to August) and the average solar radiation measured in Girona and Barcelona (June to August). In 2005,  
365 2006, 2010, 2013, 2015 and 2017, the highest EHITs at almost all the sites were recorded. Temperature and  
366 insolation seem to have a major role in the occurrence of EHITs in 2006, 2010, 2015 and 2017. The effect of  
367 heat waves on O<sub>3</sub> episodes is widely known (Solberg et al., 2008; Meehl et al., 2018; Pyrgou et al., 2018; among  
368 others). However, because the emissions of precursors have clearly decreased (–30% decrease on June to  
369 August OMI-NO<sub>2</sub> levels across the S–N axis from 2005 to 2017; –2.7% year<sup>-1</sup> with statistical significance) the  
370 number of EHITs recorded in the warmest years has probably decreased with respect to a scenario where  
371 emissions would have been maintained. In any case, some years (for example 2009 and 2016) seem to be out  
372 of line for temperature and insolation being the driving forces, and other major causes also have to be  
373 relevant, with further research needed to interpret fully interannual trends. Otero et al. (2016) found that  
374 temperature is not the main driver of O<sub>3</sub> in the South-western Mediterranean, as it is in Central Europe, but  
375 the O<sub>3</sub> levels recorded the day before (a statistical proxy for the occurrence of Millán et al. (1997)'s vertical



376 recirculation of air masses). Again, the Vic Plain sites (TON, VIC, MAN) recorded most (75%) of the EHITs  
377 reported by the AQ monitoring stations in Catalonia (25%, 34% and 16%, respectively). The higher urban  
378 pattern of MAN, as shown by the higher NO concentrations, with respect to TON, might account for both the  
379 lower exceedances and the different interannual patterns.

380 Figure 10b shows that most EHITs occurred in June and July (30% and 57%, respectively), with much less  
381 frequency in May, August and September (6%, 8% and <1%, respectively). Although temperatures are higher  
382 in August than in June, the latter registers significantly more EHITs, probably due to both the stronger solar  
383 radiation and the higher concentrations of precursors (such as NO<sub>2</sub>, see OMI-NO<sub>2</sub> and solar radiation in Figure  
384 10b).

385 Figure 10c shows that EHITs occurred mainly between Tuesday and Friday (average of 19% of occurrences per  
386 day). On weekends and Mondays, EHITs were clearly lower (average of 9% of occurrences per day) than during  
387 the rest of the week, probably due to: (i) the lower emissions of anthropogenic O<sub>3</sub> precursors (such as NO<sub>x</sub>,  
388 see OMI-NO<sub>2</sub>) during weekends and (ii) to the effect of the lower Sunday emissions in the case of the lower  
389 exceedances recorded during Mondays. During weekends and in August, OMI-NO<sub>2</sub> along the S–N axis is  
390 relatively lower (–29% weekday average and –43% in August with respect to March) following the emissions  
391 patterns associated with industrial and traffic activity that drop during vacations and weekends (Figure 10).  
392 NO<sub>x</sub> data from AQ monitoring sites follow similar patterns (not shown here).

393 Figure 10d shows that the frequency of occurrence of the EHITs at MSY (45 km north of Barcelona) is lower  
394 and earlier (maxima at 14:00 h) than at Vic Plain sites (TON, VIC, MAN). The EHITs occurred mostly at 15:00,  
395 16:00, 16:00 and 19:00 h at TON, VIC, MAN and PAR (53, 63, 72 and 105 km north of Barcelona), respectively.  
396 PAR registered not only much later EHITs, but a much lower number than TON-VIC-MAN sites, again  
397 confirming the progressive O<sub>3</sub> maxima time-shift northward of Barcelona.

398 The results in Figure 11 clearly show that during non-EHIT days, the daily O<sub>3</sub> patterns are governed by the  
399 morning–midday concentration growth driven to fumigation and photochemical production, while on EHIT  
400 days there is a later abrupt increase, with maxima being delayed as we increase the distance from Barcelona  
401 along the S–N axis. This maximal second increase of O<sub>3</sub> is clearly attributable to the influence of the transport  
402 of the plume of the BMA (horizontal transport), as the secondary NO<sub>2</sub> peak at 15:00 h (Figure 11 left bottom),  
403 and the wind patterns (see Figure S3) seem to support. The differences in the late hourly O<sub>3</sub> concentration  
404 increases in EHIT versus non-EHIT days are even more evident when calculating hourly O<sub>3</sub> slopes (hourly  
405 increments or decrements of concentrations), Figure 11 (right). The first increment (fumigation and  
406 photochemistry) makes O<sub>3</sub> levels scale up to 120 μg m<sup>–3</sup> during EHIT episodes and to nearly 100 μg m<sup>–3</sup> during  
407 non-EHIT days. In EHIT days, the later peak (transport from BMA and causing most of the 180 μg m<sup>–3</sup>  
408 exceedances) in the O<sub>3</sub> slope occurs again between 14:00 h and 20:00 h, depending on the distance to BMA,  
409 but this feature is not observed on non-EHIT days.

#### 410 **3.4. Relevance of local/regional pollution plumes in high O<sub>3</sub> episodes in NE Spain**

411 Figure 12 depicts the basic atmospheric dynamics in the study area during a typical summer day, when the  
412 atmospheric conditions are dominated by mesoscale circulations. According to the previous references,  
413 indicated in Figure 12 with enclosed numbering (coinciding with the numbering below) the following O<sub>3</sub>  
414 contributions to surface concentrations in the study area can be differentiated:

- 415 a. Vertical recirculation of O<sub>3</sub>-rich air masses, which create reservoir layers of aged pollutants.
- 416 b. Vertical fumigation of O<sub>3</sub> from the above reservoirs and the following sources aloft if the MLH growth is  
417 large enough:
  - 418 b.1. Regional external O<sub>3</sub> layers (from other regions of southern Europe, such as southern France, Italy,  
419 Portugal and Tarragona).
  - 420 b.2. High free tropospheric O<sub>3</sub> background due to hemispheric long-range transport.
  - 421 b.3. High free tropospheric O<sub>3</sub> background due to stratospheric intrusions.

- 422 c. Horizontal transport of O<sub>3</sub>. Diurnal BMA plume northward transported and channeled into the Besòs–
- 423 Congost valleys.
- 424 d. Local production of O<sub>3</sub> from precursors.

425 During summer, the intense land heating due to strong solar radiation begins early in the morning. The  
426 associated convective activity produces morning fumigation processes (b in Figure 12) that bring down O<sub>3</sub> from  
427 the reservoir layers aloft, creating sharp increases in O<sub>3</sub> concentrations in the morning (see Figure 11 and S3).  
428 The breeze transports air masses from the sea inland and creates a compensatory subsidence of aged  
429 pollutants (including O<sub>3</sub>) previously retained in reservoir and external layers and high free troposphere  
430 background aloft (Millán et al., 1997, 2000; Gangoiti et al., 2001). This subsided O<sub>3</sub> then affects the marine  
431 boundary layer and reaches the city the following day with the sea breeze, producing nearly constant O<sub>3</sub>  
432 concentrations in the city during the day (Figure S3 and Figure 9). As the breeze develops, coastal emissions  
433 and their photochemical products are transported inland, generating the BMA plume (c in Figure 12) that, in  
434 addition to the daily generated O<sub>3</sub>, also contains recirculated O<sub>3</sub> from the marine air masses. Furthermore,  
435 during the transport to the Vic Plain, new O<sub>3</sub> is produced (d in Figure 12) by the intense solar radiation and the  
436 O<sub>3</sub> precursors emitted along the way (e.g., BVOCs from vegetation, NO<sub>x</sub> from industrial and urban areas,  
437 highways).

438 This new O<sub>3</sub> gets mixed with the BMA plume and channeled northward to the S–N valleys until it reaches the  
439 Vic Plain and the southern slopes of the Pre-Pyrenees. As the BMA plume (loaded with O<sub>3</sub> and precursors)  
440 travels northward, a second increase in O<sub>3</sub> concentrations can be observed in the daily cycles of O<sub>3</sub> at these  
441 sites, (see Figure 11 and S3). This was described as the second O<sub>3</sub> peak by Millán et al. (2000).

442 The marked MLH increase in the Vic Plain compared with BMA (Soriano et al., 2001; Querol et al., 2017) may  
443 produce a preferential and intensive top-down O<sub>3</sub> transport (b in Figure 12) from upper O<sub>3</sub> layers (a, b.1, b.2  
444 and b.3 in Figure 12), contributing to high O<sub>3</sub> surface concentrations. During the sea/mountain breezes'  
445 development, some air masses are injected upward to the N and NW return flows (controlled by the synoptic  
446 circulations dominated by the high-pressure system over the Azores) aloft helped by the orography (e.g.,  
447 southern slopes of mountains) and again transported back to the coastal areas where, at late evening/night it  
448 can accumulate at certain altitudes in stably stratified layers.

449 Later, at night, land breezes returning to the coastal areas develop. Depending on the orography, these  
450 drainage flows of colder air traveling to the coastal areas can accumulate on the surface or keep flowing to  
451 the sea. The transported O<sub>3</sub> is consumed along the course of the drainage flows by deposition and titration.  
452 Next day, the cycle starts anew, producing almost closed loops enhancing O<sub>3</sub> concentrations throughout the  
453 days in the area. When the loop is active for several days, multiple O<sub>3</sub> EHITs occur over the Vic Plain.

454 The main complexity of this system arises from the fact that all these vertical/horizontal,  
455 local/regional/hemispheric/stratospheric contributions are mixed and all contribute to surface O<sub>3</sub>  
456 concentrations with different proportions that may largely vary with time and space across the study area.  
457 However, for the most intense O<sub>3</sub> episodes, the local-regional contribution might be very relevant to cause  
458 EHITs in the region. Furthermore, the intensity and frequency of O<sub>3</sub> episodes are partially driven by the  
459 occurrence of heat waves in summer and spring (Vautard et al., 2007; Gerova et al., 2007; Querol et al., 2016;  
460 Guo et al., 2017). If local and regional emissions of precursors are high, the intensity of the episodes will also  
461 be high. Thus, even though heat wave occurrences increase the severity of O<sub>3</sub> episodes, an effort to reduce  
462 precursors should be undertaken to decrease their intensity.

463 The generation of the O<sub>3</sub> episodes in 2005–2017 for the S–N corridor BMA–Vic Plain–Pre-Pyrenees occurs in  
464 atmospheric scenarios described in detail by Millán et al. (1997, 2000, 2002), Gangoiti et al. (2001), Kalabokas  
465 et al. (2007, 2008, 2017), Millán (2014) and Querol et al. (2018) for other regions of the Mediterranean basin,  
466 including Spain, or described in the same area for specific episodes (Toll and Baldasano, 2000; Gonçalves et  
467 al., 2009; Valverde et al., 2016; Querol et al., 2017). However, results from our study evidence a higher role of

468 the local-regional emissions on the occurrence of O<sub>3</sub> EHITs. Thus, our results demonstrate an increase in the  
469 EHITs northward from Barcelona to around 70 km and a decrease from there to 100 km from Barcelona  
470 following the same direction. There is also a higher frequency of occurrence of these in July (and June) and  
471 from Tuesday to Friday and a time-shift of the frequency of occurrence of EHITs from 45 to 100 km. The  
472 mountain site of MSY (located at 700 m a.s.l.) registered many fewer EHITs than the sites in the valleys (TON-  
473 VIC-MAN, 460–600 m a.s.l.) during the period, showing the key role of the valley channeling of the high O<sub>3</sub> and  
474 precursors BMA plume in July (when sea breeze and insolation are more intense). Furthermore, at the Vic  
475 Plain, we detected an inverse O<sub>3</sub> weekend effect, suggesting that local/regional anthropogenic emissions of  
476 precursors play a key role in increasing the number of EHITs on working days, with a Friday/Sunday rate of 5  
477 for VIC for 2005–2017. Despite this clear influence of the BMA plume on EHITs' occurrence, Querol et al. (2017)  
478 demonstrated that at high atmospheric altitudes (2000–3000 m a.s.l.) high O<sub>3</sub> concentrations are recorded, in  
479 many cases reaching 150 µg m<sup>-3</sup> due to the frequent occurrence of reservoir strata. As also described above,  
480 the higher growth of the MLH in TON-VIC-MAN as compared with the coastal area accounts also for higher  
481 top-down O<sub>3</sub> contributions. On the other side, close to the Pyrenees (PAR station), large forested and more  
482 humid areas give rise to a thinner MLH, hindering O<sub>3</sub> fumigation too. Furthermore, in these more distant  
483 northern regions O<sub>3</sub> consumption by ozonolysis of BVOCs might prevail over production due to weaker solar  
484 radiation during the later afternoon.

485 Figure 13 shows the distribution of average background OMI-NO<sub>2</sub> levels across the Western Mediterranean  
486 Basin in two different scenarios: when the O<sub>3</sub> levels in the Vic Plain are low (left) or high (right). To this end,  
487 we averaged the values from VIC and TON (in the Vic Plain) from all the maximum daily 8-h mean O<sub>3</sub>  
488 concentrations calculated for all the days in July within 2005–2017, and we calculated the 25th (93 out of 370  
489 days, 105 µg m<sup>-3</sup>) and 75th (93 days, 139.5 µg m<sup>-3</sup>) percentiles of all the data (P25 and P75, respectively). For  
490 both scenarios, NO<sub>2</sub> concentrations are highest around large urban and industrial areas, including Madrid,  
491 Porto, Lisbon, Barcelona, Valencia, Paris, Frankfurt, Marseille and especially the Po Valley. The shipping routes  
492 toward the Gibraltar Strait and around the Mediterranean can be observed, as well as important highways  
493 such as those connecting Barcelona to France and Lyon to Marseille. As expected, the mountain regions (the  
494 Pyrenees and the Alps) are the areas with lower NO<sub>2</sub>. Regional levels of background OMI-NO<sub>2</sub> in the P75  
495 scenario are markedly higher with hotspots intensified and spanning over broader areas. Over Spain, new  
496 hotspots (marked in yellow), such as the coal-fired power plants in Asturias (a), ceramic industries in Castelló  
497 (c) and the coal-fired power plant in Andorra, Teruel (b), appear; in the latter case, with the pollution plume  
498 being channeled along the Ebro Valley with a NW transport. Furthermore, it is important to highlight that the  
499 maxima background NO<sub>2</sub> along the eastern coastline in Spain, including the BMA, tend to exhibit some north-  
500 northwest displacement, when compared with the P25 scenario, thus pointing to the relevance of the local  
501 emissions in causing inland O<sub>3</sub> episodes.

502 These qualitative results suggest in general less synoptic forcing in Western Europe in the P75 scenario; hence,  
503 in these conditions NO<sub>2</sub> is accumulated across the region and especially around its sources. In the east coast  
504 of the Iberian Peninsula, mesoscale circulations tend to dominate, hence the northwest displacement (taking  
505 the coastal regions as a reference) of the background NO<sub>2</sub>. The bottom part of Figure 13 zooms our study area  
506 and shows the maximum daily 8-h mean O<sub>3</sub> concentrations in all the selected AQ sites averaged for both  
507 scenarios. As shown in the P75 scenario, NO<sub>2</sub> is significantly intensified across Catalonia, especially north of  
508 the BMA spreading to the Vic Plain. Comparing O<sub>3</sub> in both scenarios, in the P75 the O<sub>3</sub> levels are much higher  
509 (mostly >105 µg m<sup>-3</sup>), across the region except the urban sites in Barcelona (due to NO titration), reaching up  
510 to 154 µg m<sup>-3</sup> in the Vic Plain.

511 Conversely, in the P25 scenario, background NO<sub>2</sub> concentrations are lower, the BMA NO<sub>2</sub> spot is significantly  
512 smaller and spreads along the coastline rather than being displaced to the north-northwest. In this case,  
513 synoptic flows seem to weaken sea breeze circulations and vertical recirculation, thus reducing the amount of  
514 background NO<sub>2</sub> and the inland transport from the coast. In these conditions, O<sub>3</sub> levels are markedly lower  
515 across the territory, the RB PON site (downwind of the city/industrial area of Tarragona) being the one  
516 recording the maximum daily 8-h mean O<sub>3</sub> concentration (99 µg m<sup>-3</sup>).

### 517 3.5. Sensitivity analysis for O<sub>x</sub> using air quality monitoring data

518 We demonstrated above that the lower anthropogenic emissions of O<sub>3</sub> precursors in the BMA during  
519 weekends cause lower O<sub>3</sub> and O<sub>x</sub> levels in the Vic Plain than during working days (inverse O<sub>3</sub> weekend effect).  
520 To apply a sensitivity analysis using air quality monitoring data for the O<sub>3</sub> levels in the Vic Plain if BMA's  
521 emissions were reduced, we compared weekend O<sub>3</sub> and O<sub>x</sub> patterns with weekdays considering only data from  
522 June and July (August OMI-NO<sub>2</sub> levels are markedly lower, Figure 10b, therefore this month was not included).

523 Figure 14 shows the average O<sub>x</sub> concentrations (12:00 to 19:00 h) in TON and MAN (both AQ sites in the Vic  
524 Plain) according to the day of the week for the period considered. Data in VIC cannot be used for O<sub>x</sub> calculations  
525 due to the lack of NO<sub>2</sub> measurements. Despite the large variability in extreme values (i.e., maximum values  
526 with respect to minimum values, represented by whiskers), the interquartile range is quite constant on all the  
527 weekdays (between 13.6 to 17.3 ppb in TON and 12.7 to 19.1 in MAN). The average O<sub>x</sub> decrease between the  
528 day with highest O<sub>x</sub> levels (Wednesday in TON and Friday in MAN) and the day with the lowest O<sub>x</sub> levels  
529 (Sunday in TON and Monday in MAN) is between 6.5 (TON) and 7.7 ppb (MAN), approximately 13 and 15 μg  
530 O<sub>3</sub> m<sup>-3</sup>, 10-12% decrease). The observed decrements on O<sub>x</sub> levels downwind BMA due to the reduction in O<sub>3</sub>  
531 precursors' emissions in the BMA during weekends, can give us a first approximation of the effect that episodic  
532 mitigation measures could have on the O<sub>x</sub> or O<sub>3</sub> levels in the Vic Plain. Thus, we considered feasible a scenario  
533 with a maximum potential of O<sub>x</sub> reduction of 24.5 ppb (approximately 49 μg O<sub>3</sub> m<sup>-3</sup>, 32% decrease) when  
534 applying episodic mitigation measures (lasting 1-2 days equivalent to a weekend when, on average, NO and  
535 NO<sub>2</sub> are reduced 51 and 21%, respectively, compared with week days in the BMA monitoring sites). This was  
536 calculated as the difference between the P75 of O<sub>x</sub> values observed on Wednesdays minus the P25 of O<sub>x</sub> values  
537 on Sundays. Obviously, if these mitigation measures would be implemented structurally, instead of  
538 episodically, O<sub>x</sub> and O<sub>3</sub> decreases would be probably larger because not only the local O<sub>3</sub> coming from the  
539 BMA plume would be reduced but also the recirculated O<sub>3</sub> and thus the intensity of O<sub>3</sub> fumigation in the Plain.  
540 Therefore, it is probable that both structural and episodic measures to abate VOCs and NO<sub>x</sub> emissions in the  
541 BMA would result in evident reductions of O<sub>3</sub> in the Vic Plain, as evidenced by modeling tools by Valverde et  
542 al. (2016).

### 543 4. Conclusions

544 We analyzed 2005–2017 data sets on ozone (O<sub>3</sub>) concentrations in an area frequently affected by the  
545 northward atmospheric plume transport of Barcelona Metropolitan Area (BMA) to the Vic Plain, the area of  
546 Spain recording the highest number of exceedances of the hourly O<sub>3</sub> information threshold (EHIT, 180 μg m<sup>-3</sup>).  
547 We aimed at evaluating the potential benefits of implementing local short-term measures to abate  
548 emissions of precursors. To this end, we analyzed in detail spatial and time (interannual, weekly, daily and  
549 hourly) variations of the concentration of O<sub>3</sub> and nitrogen oxides (including remote sensing data for the latter)  
550 in April–September and built a conceptual model for the occurrence of high O<sub>3</sub> episodes. Finally, a sensitivity  
551 analysis is done with the AQ data to evaluate potential O<sub>3</sub> reductions in the North of the BMA on Sundays,  
552 compared with weekdays, as a consequence of the reduction of emissions of precursors.

553 Results showed a generalized decrease trend for regional background O<sub>3</sub> ranging from -1.1 to -1.6% year<sup>-1</sup>,  
554 as well as the well-known increase of urban O<sub>3</sub> (+0.4 to +3.2% year<sup>-1</sup>) and higher urban NO decreasing slopes  
555 than those of NO<sub>2</sub> (-2.2 to -4.3 and -1.3 to -2.0% year<sup>-1</sup>, respectively), that might account in part for the  
556 urban O<sub>3</sub> increase.

557 The most intensive O<sub>3</sub> episodes in the North of the BMA have O<sub>3</sub> contributions from relatively high regional  
558 background O<sub>3</sub> (due to a mix of continental, hemispheric–tropospheric and stratospheric contributions) as  
559 well as O<sub>3</sub> surface fumigation from the mid-troposphere high O<sub>3</sub> upper layers arising from the concatenation  
560 of the vertical recirculation of air masses (as a result of the interaction of a complex topography with intensive  
561 spring–summer sea and mountain breezes circulations (Millán et al., 1997, 2000; Gangoiti et al., 2001;  
562 Valverde et al., 2016; Querol et al., 2017). However, we noticed that for most EHIT days in the Vic Plain, the  
563 exceedance occurs when an additional contribution is added to the previous two: O<sub>3</sub> supply by the channeling  
564 of the BMA pollution plume along the S–N valley connecting BMA and Vic. Thus, despite the large external O<sub>3</sub>

565 contributions, structural and short-time local measures to abate emissions of precursors might clearly  
566 influence spring–summer O<sub>3</sub> in the Vic Plain. This is supported by (i) the reduced hourly exceedances of the O<sub>3</sub>  
567 information threshold recorded on Sundays at the Vic AQ monitoring site (9 in 2005–2017) compared with  
568 those on Fridays (47), as well as by (ii) the occurrence of a typical and marked Sunday O<sub>3</sub> pattern at the BMA  
569 AQ monitoring sites and an also marked but opposite one in the sites of the Vic Plain; and (iii) marked increase  
570 of remote sensing OMI-NO<sub>2</sub> concentrations over the BMA and northern regions during days of the P75 diurnal  
571 O<sub>3</sub> concentrations compared with those of the P25.

572 Finally, we calculated the difference between the P75 of O<sub>x</sub> diurnal concentrations recorded at two of the Vic  
573 Plain AQ monitoring stations for Wednesdays minus those of the P25 percentile of O<sub>x</sub> for Sundays, equivalent  
574 to 1–2 days of emissions reductions in the BMA. A maximum decrease potential by applying short-term  
575 measures of 24.5 ppb (approximately 49 µg O<sub>3</sub> m<sup>-3</sup>, 32% decrease) of the diurnal concentrations was  
576 calculated. Obviously, structurally implemented measures, instead of episodic ones, would result probably in  
577 important additional O<sub>x</sub> and O<sub>3</sub> abatements because not only the local O<sub>3</sub> coming from the BMA plume would  
578 be reduced but also the recirculated O<sub>3</sub>, and thus the intensity of O<sub>3</sub> fumigation on the Plain. Therefore, it is  
579 highly probable that both structural and episodic measures to abate NO<sub>x</sub> and VOCs emissions in the BMA  
580 would result in evident reductions of O<sub>3</sub> in the Vic Plain.

#### 581 **Author contributions**

582 JM performed the data compilation, treatment and analysis with the aid of XQ, CC and ME. JM, CC, ME, JB, AA  
583 and XQ contributed to the discussion and interpretation of the results. JM and XQ wrote the manuscript. JM,  
584 CC, ME, JB, AA and XQ commented on the manuscript.

#### 585 **Competing interests**

586 The authors declare that there is no conflict of interest.

#### 587 **5. Acknowledgments**

588 The present work was supported by the “Agencia Estatal de Investigación” from the Spanish Ministry of  
589 Science, Innovation and Universities and FEDER funds under the project HOUSE (CGL2016-78594-R), by the  
590 Spanish Ministerio para la Transición Ecológica (17CAES010/ Encargo) and by the Generalitat de Catalunya  
591 (AGAUR 2017 SGR41). We would like to thank the Department of Territory and Sustainability of the Generalitat  
592 de Catalunya for providing us with air quality data, and the Met Office from Catalonia (Meteocat) for providing  
593 meteorological data, as well as to NASA for providing OMI-NO<sub>2</sub> data and the ICAEN-UPC for providing solar  
594 radiation measurements. Cristina Carnerero thanks “Agencia Estatal de Investigación” for the Grant received  
595 to carry out her Ph.D. (FPI grant: BES-2017-080027).

#### 596 **6. References**

597 Ajuntament de Barcelona: Statistical yearbook of Barcelona City, Year 2010, Statistics department, Barcelona  
598 City Council, <https://bcnroc.ajuntament.barcelona.cat/jspui/handle/11703/91953>, last access: 13 April 2018,  
599 2010.

600 Ajuntament de Barcelona: Statistical yearbook of Barcelona City, Year 2017, Statistics department, Barcelona  
601 City Council, <https://bcnroc.ajuntament.barcelona.cat/jspui/handle/11703/106244>, last access: 13 April 2018,  
602 2017.

603 Baldasano, J. M., Cremades, L., and Soriano, C.: Circulation of Air Pollutants over the Barcelona Geographical  
604 Area in Summertime, in G. Angeletti and G. Restelli (eds.), Proceedings of the Sixth European Symposium on  
605 Physico-Chemical Behavior of Atmospheric Pollutants, Environmental Research Program of the European  
606 Community, Air Pollution Research Report EUR 15609/1, 474–479, 1994.

607 Carslaw, D. C. and Ropkins, K.: Openair - an R package for air quality data analysis, *Environmental Modelling &*  
608 *Software*, Volume 27-28, 52-61, 2012.

609 Carslaw, D. C., Murrells, T.P., Andersson, J., Keenan, M.: Have vehicle emissions of primary NO<sub>2</sub> peaked?,  
610 *Faraday Discussions*, Volume 189, 439-454, <https://doi.org/10.1039/C5FD00162E>, 2016.

611 DEFRA: Department for Environment Food & Rural Affaris, Conversion Factors Between ppb and µgm-3 and  
612 ppm and mgm-3, [https://uk-](https://uk-air.defra.gov.uk/assets/documents/reports/cat06/0502160851_Conversion_Factors_Between_ppb_and.pdf)  
613 [air.defra.gov.uk/assets/documents/reports/cat06/0502160851\\_Conversion\\_Factors\\_Between\\_ppb\\_and.pdf](https://uk-air.defra.gov.uk/assets/documents/reports/cat06/0502160851_Conversion_Factors_Between_ppb_and.pdf),  
614 last access: 11 February 2018, 2014.

615 Dieguez J.J., Millán M., Padilla L., Palau J.L.: Estudio y evaluación de la contaminación atmosférica por ozono  
616 troposférico en España, CEAM Report for the Ministry of Agriculture, Food and Environment, INF FIN/O3/2009,  
617 372 pp., 2009.

618 Dieguez J.J., Calatayud V., Mantilla E.: CEAM Report for the Ministry of Agriculture, Food and Environment,  
619 Fundación Biodiversidad, Informe Final, Memoria Técnica Proyecto CONOZE, CONTaminación por OZono en  
620 España, 137 pp., 2014.

621 EC: Ozone dynamics in the Mediterranean Basin: A collection of scientific papers resulting from the MECAPIP,  
622 RECAPMA and SECAP Projects, Air Pollution Report 78, DG RTD I.2, LX 46 2/82, B-1049 Brussels, 2002.

623 EC: European Commission Decision of 19 March 2004 “Concerning guidance for implementation of Directive  
624 2002/3/EC of the European Parliament and the Council relating to ozone in ambient air (2004/279/EC), Official  
625 Journal of the European Union L87/50 of 25.3.2004, 2004.

626 EC: Directive 2008/50/EC of 21 May 2008. On ambient air quality and cleaner air for Europe, Off. J. Eur. Union,  
627 11.6.2008, L152/1, <http://eur-lex.europa.eu/legal-content/ES/TXT/?uri=CELEX:32008L0050>, last access: 14  
628 December 2017, 2008.

629 EEA: Air quality in Europe – 2015 report, EEA Report, No 5/2015 (ISSN 1977-8449), 57 pp., 2015.

630 EEA: Air quality in Europe – 2016 report, EEA Report, No 28/2016 (ISSN 1977-8449), 83 pp., 2016.

631 EEA: Air quality in Europe – 2018 report, EEA Report, No 12/2018 (ISSN 1977-8449), 88 pp., 2018.

632 EMEP-CCC: Air pollution trends in the EMEP region between 1990 and 2012, EMEPCCC-Report 2016/1 102 pp.,  
633 [http://icpvegetation.ceh.ac.uk/publications/documents/EMEP\\_Trends\\_Report\\_final\\_published.pdf](http://icpvegetation.ceh.ac.uk/publications/documents/EMEP_Trends_Report_final_published.pdf), last  
634 access: 23 January 2018, 2016.

635 Finlayson-Pitts, B.J. and Pitts Jr., J.N.: Atmospheric chemistry of tropospheric ozone formation: scientific and  
636 regulatory implications, *Air Waste* 43 (8), 1091–1100, <https://doi.org/10.1080/1073161X.1993.10467187>,  
637 1993.

638 Fowler, D., Pilegaard, K., Sutton, M. A., Ambus, P., Raivonen, M., Duyzer, J., Simpson, D., Fagerli, H., Fuzzi, S.,  
639 Schjoerring, J. K., Granier, C., Neftel, A., Isaksen, I. S. A., Laj, P., Maione, M., Monks, P. S., Burkhardt, J.,  
640 Daemmgen, U., Neiryck, J., Personne, E., Wichink-Kruit, R., Butterbach-Bahl, K., Flechard, C., Tuovinen, J. P.,  
641 Coyle, M., Gerosa, G., Loubet, B., Altimir, N., Gruenhage, L., Ammann, C., Cieslik, S., Paoletti, E., Mikkelsen, T.  
642 N., Ro-Poulsen, H., Cellier, P., Cape, J. N., Horvath, L., Loreto, F., Niinemets, U., Palmer, P. I., Rinne, J., Misztal,  
643 P., Nemitz, E., Nilsson, D., Pryor, S., Gallagher, M. W., Vesala, T., Skiba, U., Brüeggemann, N., Zechmeister-  
644 Boltenstern, S., Williams, J., O’Dowd, C., Facchini, M. C., de Leeuw, G., Flossman, A., Chaumerliac, N., and  
645 Erismann, J. W.: Atmospheric composition change: Ecosystems-Atmosphere interactions, *Atmospheric*  
646 *Environment*, 43, 5193–5267, <https://doi.org/10.1016/j.atmosenv.2009.07.068>, 2009.

647 Gangoiti G., Millán M.M., Salvador R., and Mantilla E.: Long-range transport and re-circulation of pollutants in  
648 the western Mediterranean during the project Regional Cycles of Air Pollution in the West-Central  
649 Mediterranean Area, *Atmospheric Environment*, 35, 6267-6276, [https://doi.org/10.1016/S1352-](https://doi.org/10.1016/S1352-2310(01)00440-X)  
650 [2310\(01\)00440-X](https://doi.org/10.1016/S1352-2310(01)00440-X), 2001.

651 GBD: Global Burden of Disease Study 2016 Cause-Specific Mortality 1980-2016, Seattle, United States:  
652 Institute for Health Metrics and Evaluation (IHME), 2016.

653 GC: Geoinformation Air Quality information, Departament de Territori i sostenibilitat, Generalitat de  
654 Catalunya, <http://dtes.gencat.cat/icqa/start.do?lang=en>, last access: 23 February 2018, 2017a.

655 GC: Zones de qualitat de l'aire (ZQA), Departament de Territori i sostenibilitat, Generalitat de Catalunya,  
656 [http://mediambient.gencat.cat/web/.content/home/ambits\\_dactuacio/atmosfera/qualitat\\_de\\_laيرة/avaluac](http://mediambient.gencat.cat/web/.content/home/ambits_dactuacio/atmosfera/qualitat_de_laيرة/avaluacio/xarxa_de_vigilancia_i_previsio_de_la_contaminacio_atmosferica_xvpca/ZQA/Llista-de-relacio-de-municipis-i-ZQA.PDF)  
657 [io/xarxa de vigilancia i previsio de la contaminacio atmosferica\\_xvpca/ZQA/Llista-de-relacio-de-](http://mediambient.gencat.cat/web/.content/home/ambits_dactuacio/atmosfera/qualitat_de_laيرة/avaluacio/xarxa_de_vigilancia_i_previsio_de_la_contaminacio_atmosferica_xvpca/ZQA/Llista-de-relacio-de-municipis-i-ZQA.PDF)  
658 [municipis-i-ZQA.PDF](http://mediambient.gencat.cat/web/.content/home/ambits_dactuacio/atmosfera/qualitat_de_laيرة/avaluacio/xarxa_de_vigilancia_i_previsio_de_la_contaminacio_atmosferica_xvpca/ZQA/Llista-de-relacio-de-municipis-i-ZQA.PDF), last access: 23 January 2018, 2017b.

659 GC: Catalonia GHG Emissions. Catalan Office of Climate Change, Generalitat de Catalunya,  
660 [http://canviclimatic.gencat.cat/ca/politiques/inventaris\\_d\\_emissions\\_de\\_geh/emissions\\_de\\_geh\\_a\\_catalun](http://canviclimatic.gencat.cat/ca/politiques/inventaris_d_emissions_de_geh/emissions_de_geh_a_catalunya/)  
661 [ya/](http://canviclimatic.gencat.cat/ca/politiques/inventaris_d_emissions_de_geh/emissions_de_geh_a_catalunya/), last access: 13 February 2018, 2017c.

662 Gerasopoulos, E., Kouvarakis, G., Vrekoussis, M., Kanakidou, M., and Mihalopoulos, N.: Ozone variability in the  
663 marine boundary layer of the Eastern Mediterranean based on 7-year observations, *J. Geophys. Res.*, 110,  
664 D15309, <https://doi.org/10.1029/2005JD005991>, 2005.

665 Gonçalves M., Jiménez-Guerrero P., and Baldasano J.M.: Contribution of atmospheric processes affecting the  
666 dynamics of air pollution in South-Western Europe during a typical summertime photochemical episode,  
667 *Atmospheric Chemistry and Physics*, 9, 849-864, 2009.

668 Guerova, G., Jones, N.: A global model study of ozone distributions during the August 2003 heat wave in  
669 Europe, *Environmental Chemistry*, 4, 285–292, 2007.

670 Guo, Y., Gasparrini, A., Armstrong, B.G., Tawatsupa, B., Tobias, A., Lavigne, E., de Sousa Zanotti Stagliorio  
671 Coelho, M., Pan X., Kim H., Hashizume M., Honda Y., Guo Y.-L. L., Wu Ch-F., Zanobetti A., Schwartz J.D., Bell  
672 M.L., Scortichini M., Michelozzi P., Punnasiri K., Li S., Tian L., Osorio Garcia S.D., Seposo X., Overcenco A., Zeka  
673 A., Goodman P., Dang T.N., Dung D.V., Mayvaneh F., Saldiva P.H.N., Williams G., Tong S.: Temperature  
674 variability and mortality: a multi-country study, *Environmental Health Perspectives* 124, 1554, 2016.

675 Hewitt, C. N., Ashworth, K., Boynard, A., Guenther, A., Langford, B., MacKenzie, A. R., Misztal, P. K., Nemitz, E.,  
676 Owen, S. M., Possell, M., Pugh, T. A. M., Ryan, A. C., and Wild, O.: Groundlevel ozone influenced by circadian  
677 control of isoprene emissions, *Nature Geoscience*, 4, 671–674, <https://doi.org/10.1038/ngeo1271>, 2011.

678 ICAEN-UPC: Xarxa de Mesura de la Irradiància Solar a Catalunya, 2018.

679 IPCC: Climate Change 2013, The Physical Science Basis, Working Group I Contribution to the Fifth Assessment  
680 Report of the Intergovernmental Panel on Climate Change, edited by: Stocker T.F., Qin D., Plattner G.-K., Tignor  
681 M.M.B., Allen S.K., Boschung J., Nauels A., Xia Y., Bex V., Midgley P.M., Cambridge University Press, Cambridge,  
682 United Kingdom and New York, NY, USA. <http://www.ipcc.ch/report/ar5/wg1/>, last access: 23 January 2018,  
683 2013.

684 Jacob, D., Winner, D.: Effect of climate change on air quality, *Atmospheric Environment* 43(1): 51-63,  
685 <http://nrs.harvard.edu/urn-3:HUL.InstRepos:3553961>, last access: 23 January 2018, 2009.

686 Jiménez, P. and Baldasano, J.M.: Ozone response to precursor controls in very complex terrains: use of  
687 photochemical indicators to assess O<sub>3</sub>-NO<sub>x</sub>-VOC sensitivity in the northeastern Iberian Peninsula, *Journal of*  
688 *Geophysical Research* 109, D20309, <https://doi.org/10.1029/2004JD00498>, 2004.

689 Kalabokas, P.D., Volz-Thomas, A., Brioude, J., Thouret, V., Cammas, J.-P., and Repapis, C. C.: Vertical ozone  
690 measurements in the troposphere over the Eastern Mediterranean and comparison with Central Europe,  
691 *Atmospheric Chemistry and Physics*, 7, 3783–3790, <https://doi.org/10.5194/acp-7-3783-2007>, 2007.

692 Kalabokas P.D., Mihalopoulos N., Ellul R., Kleanthous S., Repapis C.C: An investigation of the meteorological  
693 and photochemical factors influencing the background rural and marine surface ozone levels in the Central  
694 and Eastern Mediterranean, *Atmospheric Environment*, 42, 7894-7906, 2008.

695 Kalabokas P.D., Hjorth J., Foret G., Dufour G., Eremenko M., Siour G., Cuesta J., Beekmann M.: An investigation  
696 on the origin of regional springtime ozone episodes in the western Mediterranean, *Atmos. Chem. Phys.* 17,  
697 3905–3928, 2017.

698 Kley, D. and Geiss, H.: Tropospheric ozone at elevated sites and precursor emissions in the United States and  
699 Europe, *Atmospheric Environment*, 8, 149–158, 1994.

700 Krotkov, N. and Veefkind, P.: OMI/Aura Nitrogen Dioxide (NO<sub>2</sub>) Total and Tropospheric Column 1-orbit L2  
701 Swath 13x24 km V003, Greenbelt, MD, USA, Goddard Earth Sciences Data and Information Services Center  
702 (GES DISC), <https://doi.org/10.5067/Aura/OMI/DATA2017>, 2016.

703 Lelieveld J., Berresheim H., Borrmann S., Crutzen P.J., Dentener F.J., Fischer H., Feichter J., Flatau P.J., Heland  
704 J., Holzinger R., Kormann R., Lawrence M.G., Levin Z., Markowicz K.M., Mihalopoulos N., Minikin A.,  
705 Ramanathan V., de Reus M., Roelofs G.J., Scheeren H.A., Sciare J., Schlager H., Schultz M., Siegmund P., Steil  
706 B., Stephanou E.G., Stier P., Traub M., Warneke C., Williams J., Ziereis H.: Global air pollution crossroads over  
707 the Mediterranean, *Science*, 298, 794-799, 2002.

708 Logan, J. A.: Tropospheric ozone – seasonal behaviour, trends, and anthropogenic influence, *Journal of*  
709 *Geophysical Research: Atmospheres*, 90, 10463– 10482, 1985.

710 Mantilla E., Millán M.M., Sanz M.J., Salvador R., and Carratalá A.: Influence of mesometeorological processes  
711 on the evolution of ozone levels registered in the Valencian Community, In: I Technical workshop on ozone  
712 pollution in southern Europe, Valencia, 1997.

713 McLinden, C. A., Olsen, S. C., Hannegan, B., Wild, O., Prather, M. J., and Sundet, J.: Stratospheric ozone in 3-D  
714 models: A simple chemistry and the cross-tropopause flux, *Journal of Geophysical Research: Atmospheres*,  
715 105, 14653–14665, <https://doi.org/10.1029/2000jd900124>, 2000.

716 Meehl G.A., Tebaldi C., Tilmes S., Lamarque J.F., Bates S.: Future heat waves and surface ozone, *Environmental*  
717 *Research Letters* 13 064004, <https://doi.org/10.1088/1748-9326/aabcdc>, 2018.

718 Meteocat: Meteorological Office of Catalonia, Request of meteorological data reports,  
719 <http://www.meteo.cat/wpweb/serveis/peticions-de-dades/peticio-dinformes-meteorologics/>, last access: 23  
720 January 2018) and <http://meteocat.gencat.cat/observacions/llistat-xema>, last access: 6 December 2017, 2017.

721 MFom: Ministerio de Fomento: Áreas urbanas en España 2017, Dirección General de Arquitectura, Vivienda y  
722 Suelo, <http://atlasau.fomento.gob.es>, last access: 6 December 2017, 2017.

723 Millán M.M.: El ozono troposférico en el sur de Europa: aspectos dinámicos documentados en proyectos  
724 europeos, CEAM Report for the Ministry of Agriculture, Food and Environment, INF FIN/O3/2009(annex), 156  
725 pp., [http://www.mapama.gob.es/es/calidad-y-evaluacion-ambiental/temas/atmosfera-y-calidad-del-](http://www.mapama.gob.es/es/calidad-y-evaluacion-ambiental/temas/atmosfera-y-calidad-del)



- 726 [aire/Ozono%20Troposf%C3%A9rico%20en%20el%20sur%20de%20Europa-Actualizacion-2009\\_tcm30-](https://www.tcm30-187999.pdf)  
727 [187999.pdf](https://www.tcm30-187999.pdf), last access: 13 February 2018, 2009.
- 728 Millán M.M.: Extreme hydrometeorological events and climate change predictions in Europe, *J. Hydrol.* 518B,  
729 206-224, 2014.
- 730 Millán M.M., Salvador R., Mantilla E., and Kallos G.: Photooxidant dynamics in the Mediterranean basin in  
731 summer: Results from European research projects, *Journal of Geophysical Research* 102, 8811-8823, 1997.
- 732 Millán M.M., Mantilla E., Salvador R., Carratalá A., Sanz M.J., Alonso L., Gangoiti G., and Navazo M.: Ozone  
733 Cycles in the Western Mediterranean Basin: Interpretation of Monitoring Data in Complex Coastal Terrain,  
734 *Journal of Applied Meteorology*, 39: 487-508, 2000.
- 735 Millán M.M., Sanz M.J., Salvador R., and Mantilla E.: Atmospheric dynamics and ozone cycles related to  
736 nitrogen deposition in the western Mediterranean. *Environmental Pollution*, 118, 167-186, 2002.
- 737 Monks P.S., Archibald A.T., Colette A., Cooper O., Coyle M., Derwent R., Fowler D., Granier C., Law K.S., Mills  
738 G.E., Stevenson D.S., Tarasova O., Thouret V., von Schneidemesser E., Sommariva R., Wild O., Williams M.L.:  
739 Tropospheric ozone and its precursors from the urban to the global scale from air quality to short-lived climate  
740 forcer, *Atmospheric Chemistry and Physics*, 15, 8889-8973, 2015.
- 741 Olson, J. R., Crawford, J. H., Davis, D. D., Chen, G., Avery, M. A., Barrick, J. D. W., Sachse, G. W., Vay, S. A.,  
742 Sandholm, S. T., Tan, D., Brune, W. H., Faloon, I. C., Heikes, B. G., Shetter, R. E., Lefer, B. L., Singh, H. B., Talbot,  
743 R. W., and Blake, D. R.: Seasonal differences in the photochemistry of the South Pacific: A comparison of  
744 observations and model results from PEM-Tropics A and B, *Journal of Geophysical Research*, 106, 32749–  
745 32766, 2001.
- 746 OMI Team: Ozone Monitoring Instrument (OMI) Data User's Guide,  
747 [https://docserver.gesdisc.eosdis.nasa.gov/repository/Mission/OMI/3.3\\_ScienceDataProductDocumentation/  
748 3.3.2\\_ProductRequirements\\_Designs/README.OMI\\_DUG.pdf](https://docserver.gesdisc.eosdis.nasa.gov/repository/Mission/OMI/3.3_ScienceDataProductDocumentation/3.3.2_ProductRequirements_Designs/README.OMI_DUG.pdf), last access: 2 January 2018, 2012.
- 749 Otero N., Sillmann J., Schnell J. L., Rust H.W., Butler T.: Synoptic and meteorological drivers of extreme ozone  
750 concentrations over Europe, *Environ. Res. Lett.*, 11, 24005, <https://doi.org/10.1088/1748-9326/11/2/024005>,  
751 2016.
- 752 Paoletti, E., De Marco, A., Beddows, D. C. S., Harrison, R. M., & Manning, W. J.: Ozone levels in European and  
753 USA cities are increasing more than at rural sites, while peak values are decreasing, *Environmental Pollution*,  
754 192(x), 295–299, <https://doi.org/10.1016/j.envpol.2014.04.040>, 2014.
- 755 Pay, M. T., Gangoiti, G., Guevara, M., Napelenok, S., Querol, X., Jorba, O., Pérez García-Pando, C.: Ozone source  
756 apportionment during peak summer events over southwestern Europe, *Atmospheric Chemistry and Physics  
757 Discussions*, 2018, 1-43, <https://doi.org/10.5194/acp-2018-727>, 2018.
- 758 Pusede, S. E., Steiner, A.L., Cohen, R.C.: Temperature and recent trends in the chemistry of continental surface  
759 ozone, *Chemical Reviews*, 115, 3898–3918, 2015.
- 760 Pyrgou A., Hadjinicolaou P., Santamouris M.: Enhanced near-surface ozone under heatwave conditions in a  
761 Mediterranean island, *Scientific Reports* 8, 9191, <https://doi.org/10.1038/s41598-018-27590-z>, 2018.
- 762 Querol X., Alastuey A., Orío A., Pallares M., Reina F., Dieguez J. J., Mantilla E., Escudero M., Alonso L., Gangoiti  
763 G., Millán M.: On the origin of the highest ozone episodes in Spain, *Science of the Total Environment*, 572,  
764 379-389, 2016.

765 Querol X., Gangoiti G., Mantilla E., Alastuey A., Minguillón M. C., Amato F., Reche C., Viana M., Moreno T.,  
766 Karanasiou A., Rivas I., Pérez N., Ripoll A., Brines M., Ealo M., Pandolfi M., Lee H.-K., Eun H.-R., Park Y.-H.,  
767 Escudero M., Beddows D., Harrison R.M., Bertrand A., Marchand N., Lyasota A., Codina B., Olid M., Udina M.,  
768 Jiménez-Esteve B., Soler M. R., Alonso L., Millán M., Ahn, K.-H.: Phenomenology of high-ozone episodes in NE  
769 Spain, *Atmospheric Chemistry and Physics*, 17, 2817-2838, 2017.

770 Querol, X., Alastuey, A., Gangoiti, G., Perez, N., Lee, H. K., Eun, H. R. Park, Y. Mantilla, E. Escudero, M. Titos,  
771 G. Alonso, L. Temime-Roussel, B. March, N. Moreta, J. R. Revuelta, M. A. Salvador, P. Artiñano, B. García  
772 dos Santos, S. Anguas, M. Notario, A. Saiz-Lopez, A. Harrison, R. M. Ahn, K.-H.: Phenomenology of summer  
773 ozone episodes over the Madrid Metropolitan Area, central Spain, *Atmospheric Chemistry and Physics*  
774 *Discussions*, 2017, 1–38, <https://doi.org/10.5194/acp-2017-1014>, 2018.

775 Safieddine, S., Boynard, A., Coheur, P.-F., Hurtmans, D., Pfister, G., Quennehen, B., Thomas, J. L., Raut, J.-C.,  
776 Law, K. S., Klimont, Z., Hadji-Lazaro, J., George, M., and Clerbaux, C.: Summertime tropospheric ozone  
777 assessment over the Mediterranean region using the thermal infrared IASI/MetOp sounder and the WRF-  
778 Chem model, *Atmospheric Chemistry and Physics*, 14, 10119-10131, 2014.

779 Salvador R., Millán M.M., Mantilla E., and Baldasano J.M.: Mesoscale modelling of atmospheric processes over  
780 the western Mediterranean area during summer. *International Journal of Environment and Pollution*, 8, 513-  
781 528.14, 10119-10131, <https://doi.org/10.5194/acp-14-10119-2014>, 1997.

782 Sen, P. K.: Estimates of regression coefficient based on Kendall's tau, *Journal of the American Statistical*  
783 *Association* 63(324), 1968.

784 Sicard, P., De Marco, A., Troussier, F., Renou, C., Vas, N., Paoletti, E.: Decrease in surface ozone concentrations  
785 at Mediterranean remote sites and increase in the cities, *Atmospheric Environment*, 79, 705-715, 2013.

786 Solberg S., Hov Ø., Søvde A., Isaksen I.S.A., Coddeville P., De Backer H., Forster C., Orsolini Y., Uhse K.:  
787 European surface ozone in the extreme summer 2003, *Journal of Geophysical Research*, 113, D07307,  
788 <https://doi.org/10.1029/2007JD009098>, 2008.

789 Soriano, C., Baldasano, J.M., Buttler, W.T., Moore, K.: Circulatory patterns of air pollutants within the  
790 Barcelona air basin in a summertime situation: lidar and numerical approaches, *Boundary-Layer Meteorology*  
791 98 (1), 33–55, 2001.

792 Stein A.F., Mantilla E., and Millán M.M.: Ozone formation downwind an industrial complex in the western  
793 Mediterranean, In: 13th World Clean Air and Environmental Protection, August 22-27. London, U.K., 2004.

794 Stevenson, D. S., Dentener, F. J., Schultz, M. G., Ellingsen, K., van Noije, T. P. C., Wild, O., Zeng, G., Amann, M.,  
795 Atherton, C. S., Bell, N., Bergmann, D. J., Bey, I., Butler, T., Cofala, J., Collins, W. J., Derwent, R. G., Doherty, R.  
796 M., Drevet, J., Eskes, H. J., Fiore, A. M., Gauss, M., Hauglustaine, D. A., Horowitz, L. W., Isaksen, I. S. A., Krol,  
797 M. C., Lamarque, J. F., Lawrence, M. G., Montanaro, V., Muller, J. F., Pitari, G., Prather, M. J., Pyle, J. A., Rast,  
798 S., Rodriguez, J. M., Sanderson, M. G., Savage, N. H., Shindell, D. T., Strahan, S. E., Sudo, K., and Szopa, S.:  
799 Multimodel ensemble simulations of present-day and near-future tropospheric ozone, *Journal of Geophysical*  
800 *Research: Atmospheres*, 111, D08301, <https://doi.org/10.1029/2005jd006338>, 2006.

801 Theil, H.: A rank invariant method of linear and polynomial regression analysis, i, ii, iii, *Proceedings of the*  
802 *Koninklijke Nederlandse Akademie Wetenschappen, Series A - Mathematical Sciences* 53, 386-392, 521-525,  
803 1397-1412, 1950.

804 Toll, I. and Baldasano, J. M.: Modeling of photochemical air pollution in the Barcelona area with highly  
805 disaggregated anthropogenic and biogenic emissions, *Atmospheric Environment*, 34(19), 3069–3084,  
806 [https://doi.org/10.1016/S1352-2310\(99\)00498-7](https://doi.org/10.1016/S1352-2310(99)00498-7), 2000.

807 UNECE: Hemispheric transport of air pollution 2010, Part A: ozone and particulate matter, Air pollution studies,  
808 17, UNECE, LRTAP, Task Force on Hemispheric Transport of Pollutants HTAP 2010: Part A. Ozone and  
809 Particulate Matter, 278 pp, ECE/EB.AIR/100, ISBN 978-92-1-117043-6  
810 [http://www.htap.org/publications/2010\\_report/2010\\_Final\\_Report/HTAP%202010%20Part%20A%2011040](http://www.htap.org/publications/2010_report/2010_Final_Report/HTAP%202010%20Part%20A%20110407.pdf)  
811 [7.pdf](http://www.htap.org/publications/2010_report/2010_Final_Report/HTAP%202010%20Part%20A%20110407.pdf), last access: 3 November 2017, 2010.

812 Valverde V., Pay M.T., Baldasano J.M.: Ozone attributed to Madrid and Barcelona on-road transport emissions:  
813 Characterization of plume dynamics over the Iberian Peninsula, Science of the Total Environment, 543, 670–  
814 682, 2016.

815 Vautard, R., Beekmann, M., Desplat, J., Hodzic, A., & Morel, S.: Air quality in Europe during the summer of  
816 2003 as a prototype of air quality in a warmer climate, Comptes Rendus - Geoscience, 339(11–12), 747–763,  
817 <https://doi.org/10.1016/j.crte.2007.08.003>, 2007.

818 WHO: Air Quality Guidelines: Global Update 2005. Particulate matter, ozone, nitrogen dioxide and sulfur  
819 dioxide, World Health Organisation, Copenhagen, ISBN 92 890 2192 6, 484 pp.,  
820 [http://www.euro.who.int/\\_data/assets/pdf\\_file/0005/78638/E90038.pdf](http://www.euro.who.int/_data/assets/pdf_file/0005/78638/E90038.pdf), last access: 23 November 2017,  
821 2006.

822 WHO Regional Office for Europe: Review of evidence on health aspects of air pollution—REVIHAAP project:  
823 technical report, WHO Regional Office for Europe, Copenhagen 302 pp.,  
824 [http://www.euro.who.int/\\_data/assets/pdf\\_file/0004/193108/REVIHAAP-Final-technical-report-final-](http://www.euro.who.int/_data/assets/pdf_file/0004/193108/REVIHAAP-Final-technical-report-final-version.pdf?ua=1)  
825 [version.pdf?ua=1](http://www.euro.who.int/_data/assets/pdf_file/0004/193108/REVIHAAP-Final-technical-report-final-version.pdf?ua=1), last access: 23 January 2018, 2013a.

826 WHO Regional Office for Europe: Health Risks of Air Pollution in Europe—HRAPIE Project: Recommendations  
827 for Concentration-Response Functions for Cost–Benefit Analysis of Particulate Matter, Ozone and Nitrogen  
828 Dioxide, Copenhagen, 65 pp.,  
829 [http://www.euro.who.int/\\_data/assets/pdf\\_file/0017/234026/e96933.pdf?ua=1](http://www.euro.who.int/_data/assets/pdf_file/0017/234026/e96933.pdf?ua=1), last access: 23 January  
830 2018, 2013b.

831 Young, P. J., Archibald, A. T., Bowman, K. W., Lamarque, J.-F., Naik, V., Stevenson, D. S., Tilmes, S., Voulgarakis,  
832 A., Wild, O., Bergmann, D., Cameron-Smith, P., Cionni, I., Collins, W. J., Dalsøren, S. B., Doherty, R. M., Eyring,  
833 V., Faluvegi, G., Horowitz, L. W., Josse, B., Lee, Y. H., MacKenzie, I. A., Nagashima, T., Plummer, D. A., Righi, M.,  
834 Rumbold, S. T., Skeie, R. B., Shindell, D. T., Strode, S. A., Sudo, K., Szopa, S., and Zeng, G.: Preindustrial to end  
835 21st century projections of tropospheric ozone from the Atmospheric Chemistry and Climate Model  
836 Intercomparison Project (ACCMIP), Atmospheric Chemistry and Physics, 13, 2063 – 2090,  
837 <https://doi.org/10.5194/acp-13-2063-2013>, 2013.

838

839

840 **FIGURE CAPTIONS**

841 Figure 1. Location and main topographic features of the area of study.

842 Figure 2. Location (left) and main characteristics (right) of the selected air quality monitoring sites (S–N axis:  
843 green squares on the map and shaded gray on the table, rest of stations: white squares) and  
844 meteorological/solar radiation stations (red circles) selected for this study. Types of air quality monitoring sites  
845 are urban (traffic or background: UT, UB), suburban (traffic, industrial or background: SUT, SUI, SUB) and rural  
846 (background or industrial: RB, RI). PLR (Palau Reial air quality monitoring site) and BCN (Barcelona)  
847 meteorological and solar radiation sites are closely located.

848 Figure 3. Spatial variability of mean June–August O<sub>3</sub> (a) and O<sub>x</sub> (b) concentrations from 12:00 to 19:00 h  
849 observed in selected air quality monitoring sites. Data from Ciutadella (CTL), Palau Reial (PLR), Montcada  
850 (MON), Granollers (GRA), Montseny (MSY), Tona (TON), Vic (VIC), Manlleu (MAN), Pardines (PAR), Montsec  
851 (MSC), Begur (BEG), Bellver de Cerdanya (BdC), Berga (BER), Agullana (AGU), Santa Pau (STP), Mataró (MAT),  
852 Manresa (MNR), Ponts (PON), Sort (SOR), Juneda (JUN), La Sénia (LSE), Constantí (CON), Gandesa (GAN),  
853 Vilanova i la Geltrú (VGe) and Alcover (ALC) air quality monitoring stations.

854 Figure 4. Results of the time trend assessment carried out for annual season averages (April–September) of  
855 NO (a), NO<sub>2</sub> (b), O<sub>3</sub> (c & d) and O<sub>x</sub> (e) levels using the Theil–Sen statistical estimator shown graphically. Only  
856 shown the trends with statistical significance. (d) Numerical results; the symbols shown for the p-values  
857 related to how statistically significant the trend estimate is: p < 0.001 = \*\*\* (highest statistical significance), p  
858 < 0.01 = \*\* (mid), p < 0.05 = \* (moderate), p < 0.1 = + (low). No symbol means lack of significant trend. Units  
859 are µg m<sup>-3</sup>. Shaded air quality monitoring sites belong to the S–N axis. Types of air quality monitoring sites are  
860 urban (traffic or background: UT, UB), suburban (traffic, industrial or background: SUT, SUI, SUB) and rural  
861 (background: RB). Data from AQ stations with at least 10 years of valid data within the period.

862 Figure 5. (a) Annual average traffic entering Barcelona City during weekdays (weekends not considered) during  
863 2005–2016 versus GHG emissions (attributed to industry and power generation sectors) in Catalonia during  
864 2005–2016. (b) Annual NO<sub>x</sub> measured at CTL (Ciutadella) and MON (Montcada) air quality monitoring sites  
865 versus annual OMI-NASA’s measured background NO<sub>2</sub> during 2005–2017.

866 Figure 6. Monthly hourly average concentrations of O<sub>3</sub> (a) and O<sub>x</sub> (b) along the S–N axis during 2005–2017.  
867 Data from Ciutadella (CTL), Montcada (MON), Granollers (GRA), Montseny (MSY), Tona (TON), Vic (VIC),  
868 Manlleu (MAN) and Pardines (PAR) air quality monitoring stations.

869 Figure 7. Monthly weekday average concentrations of O<sub>3</sub> concentrations calculated between 12:00 and 19:00  
870 h along the S–N axis during 2005–2017. Data from Ciutadella (CTL), Montcada (MON), Granollers (GRA),  
871 Montseny (MSY), Tona (TON), Vic (VIC), Manlleu (MAN) and Pardines (PAR) air quality monitoring stations.

872 Figure 8. Weekday (W) (Monday to Friday in the BMA and Tuesday to Friday in the Vic Plain) to Weekend (WE)  
873 pollutant concentrations (O<sub>3</sub>, NO and NO<sub>2</sub>) measured at AQ sites and background NO<sub>2</sub> (remote sensing OMI)  
874 for June to August, per year along the period 2005–2017. O<sub>3</sub> concentrations (top plot) are averaged from 12:00  
875 to 19:00 h LT hourly concentrations, and NO and NO<sub>2</sub> concentrations are calculated from daily averages,  
876 including OMI-NO<sub>2</sub>. Each short line depicts the increasing or decreasing tendency of weekday concentrations  
877 (left side of each short line) with respect to weekend levels (right side of the short line). Thus, a horizontal line  
878 would represent same pollutant levels along the week (concentration in W = concentration in WE). We  
879 consider BMA AQ sites: CTL, MON and GRA and Vic Plain AQ sites: TON and MAN. The continuous lines show  
880 the percentage of variation of pollutant levels during weekends with respect to weekdays: increasing (>0) or  
881 decreasing (<0) i.e. a quantification of the inclination of each short line.  
882

883 Figure 9. (a) July O<sub>3</sub> and (b) O<sub>x</sub> daily cycles plotted from mean hourly concentrations measured in air quality  
884 monitoring sites located along the S–N axis during 2005–2017. The black arrows point to the O<sub>3</sub> and O<sub>x</sub> maxima

885 time of the day. Data from Ciutadella (CTL), Montcada (MON), Granollers (GRA), Montseny (MSY), Tona (TON),  
886 Vic (VIC), Manlleu (MAN) and Pardines (PAR) air quality monitoring stations.

887 Figure 10. For the period 2005–2017, trends of the EHITs measured by air quality monitoring stations along  
888 the S–N axis (a) Annual trends of the EHITs, average temperatures measured in Vic (Gurb) (July during 13:00  
889 to 16:00 h), background NO<sub>2</sub> measured by OMI-NASA (June to August) and average solar radiation measured  
890 at Girona and Barcelona (June to August). (b) Monthly patterns of the EHITs, average temperatures measured  
891 in Vic, background NO<sub>2</sub> measured by OMI and solar radiation measured at Girona and Barcelona. (c) Weekly  
892 patterns of the EHITs and background NO<sub>2</sub> measured by OMI. (d) Hourly patterns of the EHITs. Despite the  
893 incomplete data availability in MAN 2005, almost 20 EHITs were recorded. AQ data from Ciutadella (CTL),  
894 Montcada (MON), Granollers (GRA), Montseny (MSY), Tona (TON), Vic (VIC), Manlleu (MAN) and Pardines  
895 (PAR) monitoring stations.

896 Figure 11. Average hourly O<sub>3</sub> concentrations for all days with EHIT records and those without for Tona (TON),  
897 Vic (VIC), Manlleu (MAN) and Pardines (PAR) air quality monitoring stations, (left top) as well as for the NO<sub>2</sub>  
898 levels at TON (left bottom). Average hourly increments of O<sub>3</sub> concentrations for all days with and without EHIT  
899 records (right); in all cases for June–August 2005–2017.

900 Figure 12. Idealized two-dimensional section of O<sub>3</sub> circulations in the coastal region of Barcelona to the Pre-  
901 Pyrenees on a typical summer day (upper) and night (bottom). The gray shaded shape represents a  
902 topographic profile south to north direction, from the Mediterranean Sea to the south slopes of the Pre-  
903 Pyrenean Ranges (i.e., along the S–N axis). The colored dots and abbreviations depict the air quality monitoring  
904 stations located along the S–N axis: Ciutadella (CTL), Montcada (MON), Granollers (GRA), Montseny (MSY),  
905 Tona (TON), Vic (VIC), Manlleu (MAN) and Pardines (PAR). Modified and adapted to the S–N axis from Millán  
906 et al. (1997, 2000), Querol et al. (2017, 2018).

907 Figure 13. Daily average background NO<sub>2</sub> levels in Western Europe (top) and Catalonia (bottom), July 2005–  
908 2017 in two different scenarios. (Left) P25: days when the maximum daily 8-h mean O<sub>3</sub> concentrations in the  
909 Vic Plain are below the percentile 25 (<105 μg m<sup>-3</sup>) and (right) P75: same but concentrations being above the  
910 percentile 75 (>139.5 μg m<sup>-3</sup>).

911 Figure 14. Box plots of O<sub>x</sub> measured in TON and MAN (12:00 to 19:00h) per weekday June and July 2005–2017  
912 for those days with  $\delta O_{x, \text{TON-CTL}} > 0$  (n = 545 for TON and n = 479 for MAN of valid data). Each box represents  
913 the central half of the data between the lower quartile (P25) and the upper quartile (P75). The lines across the  
914 box displays the median values. The whiskers that extend from the bottom and the top of the box represent  
915 the extent of the main body of data. The outliers are represented by black points.

916  
917

918

919

920

921

922

923

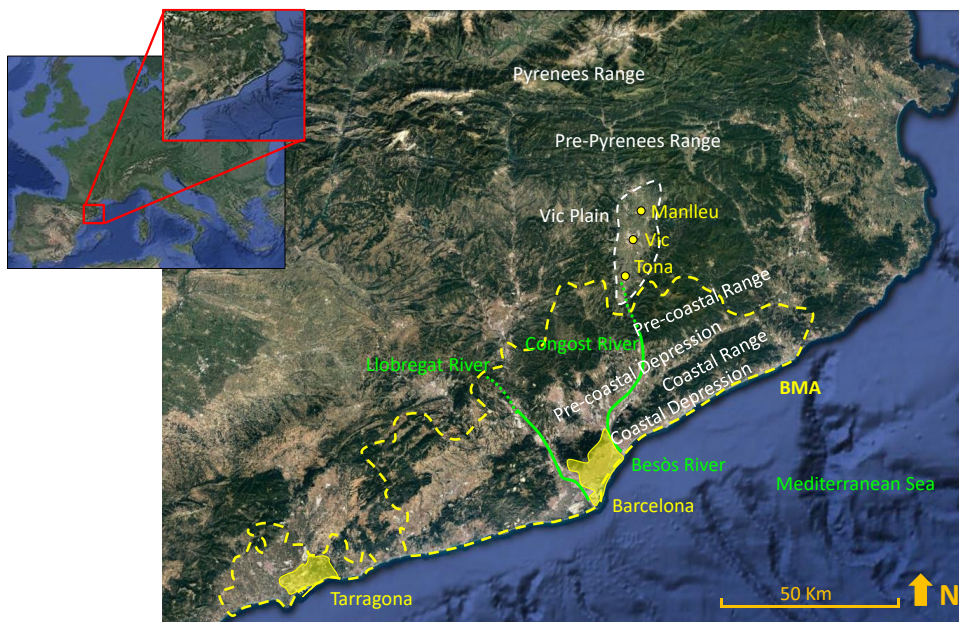
924

925

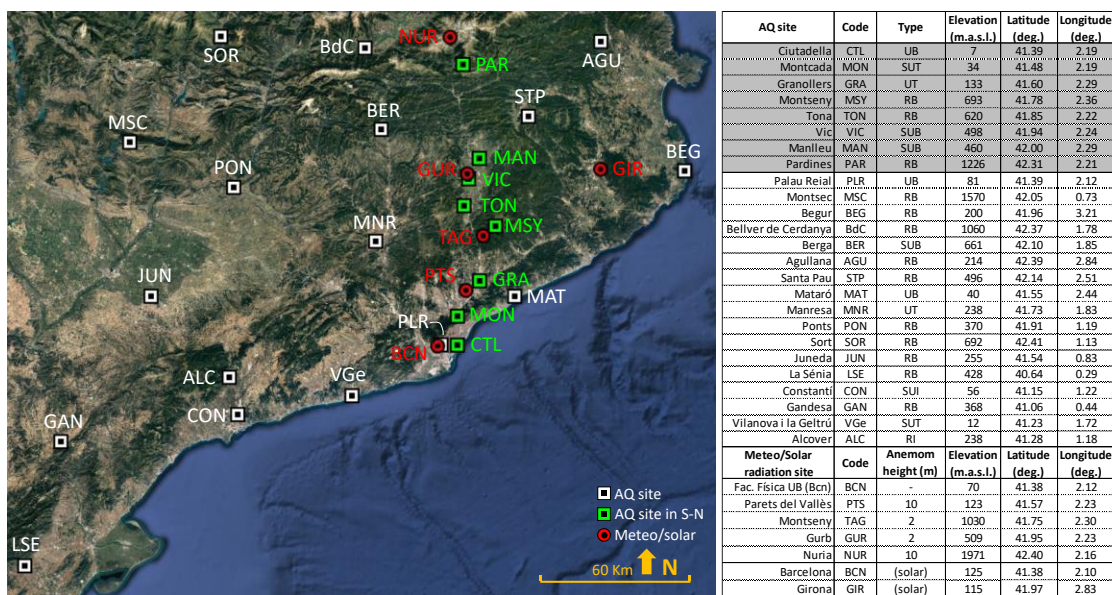
926

927 FIGURES

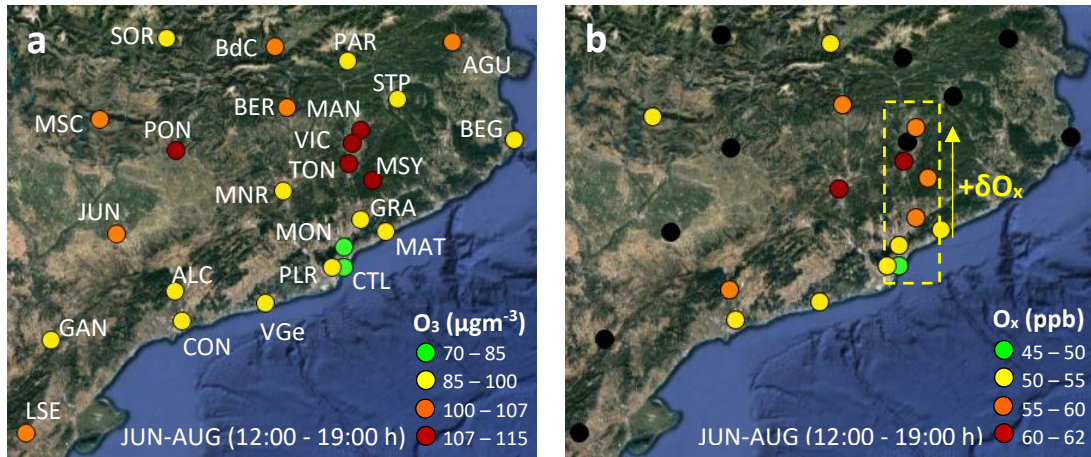
928  
929  
930  
931  
932  
933  
934  
935  
936  
937  
938  
939  
940  
941  
942  
943  
944



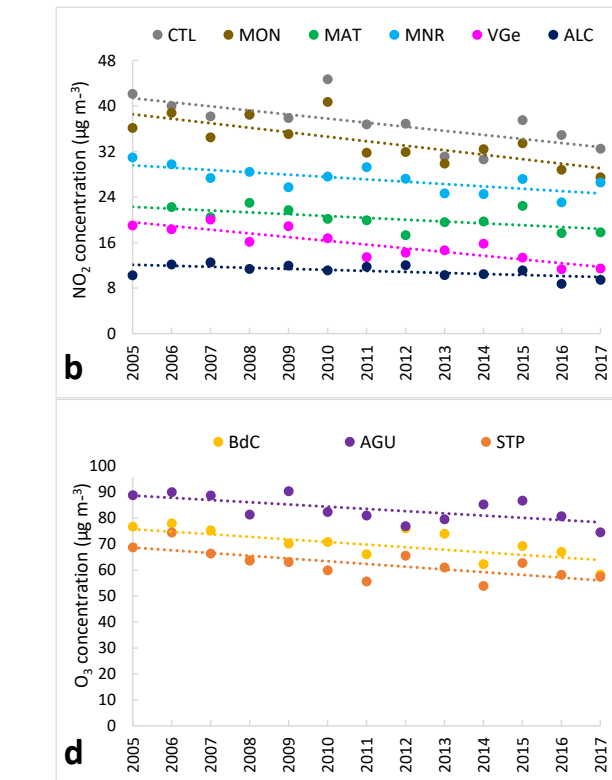
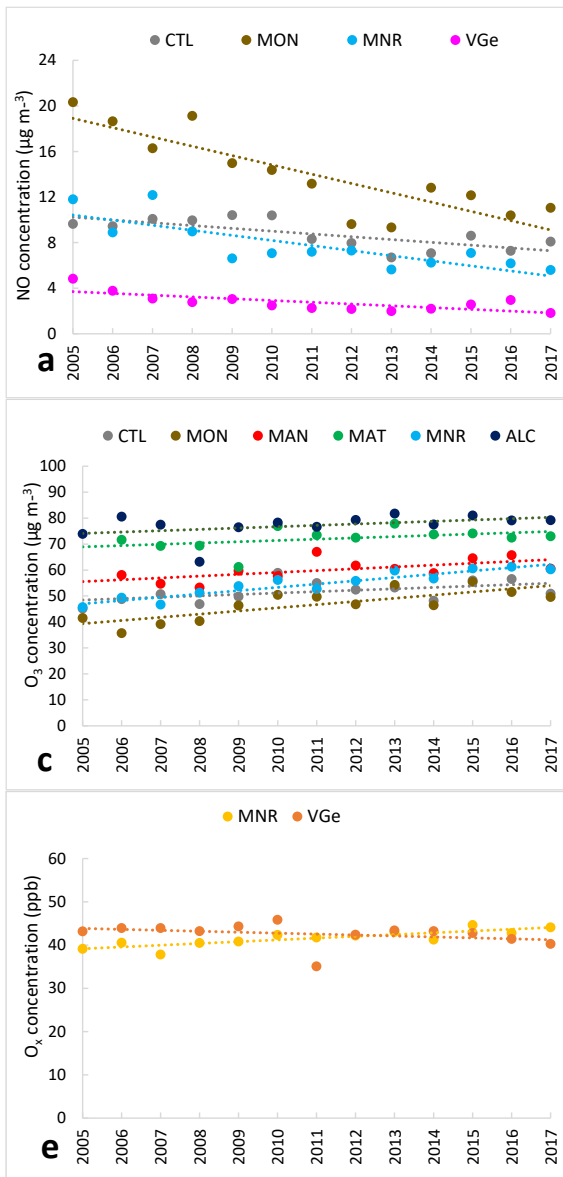
945 Figure 1



946 Figure 2

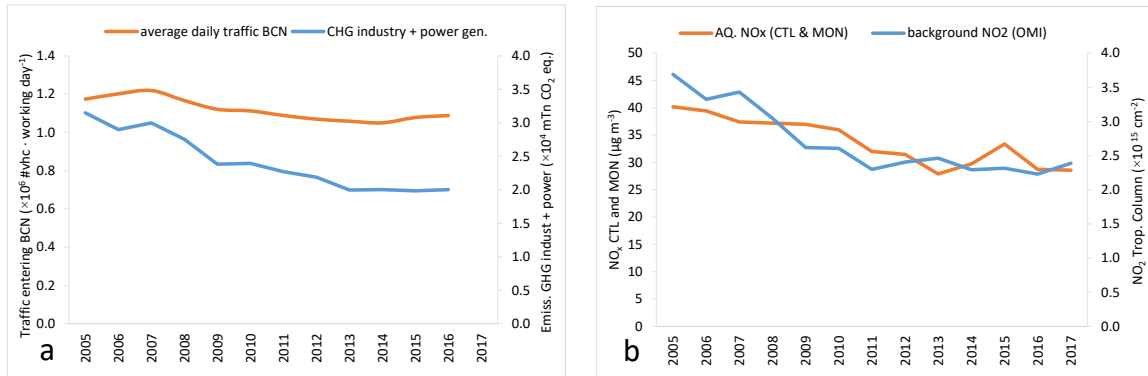


947 Figure 3

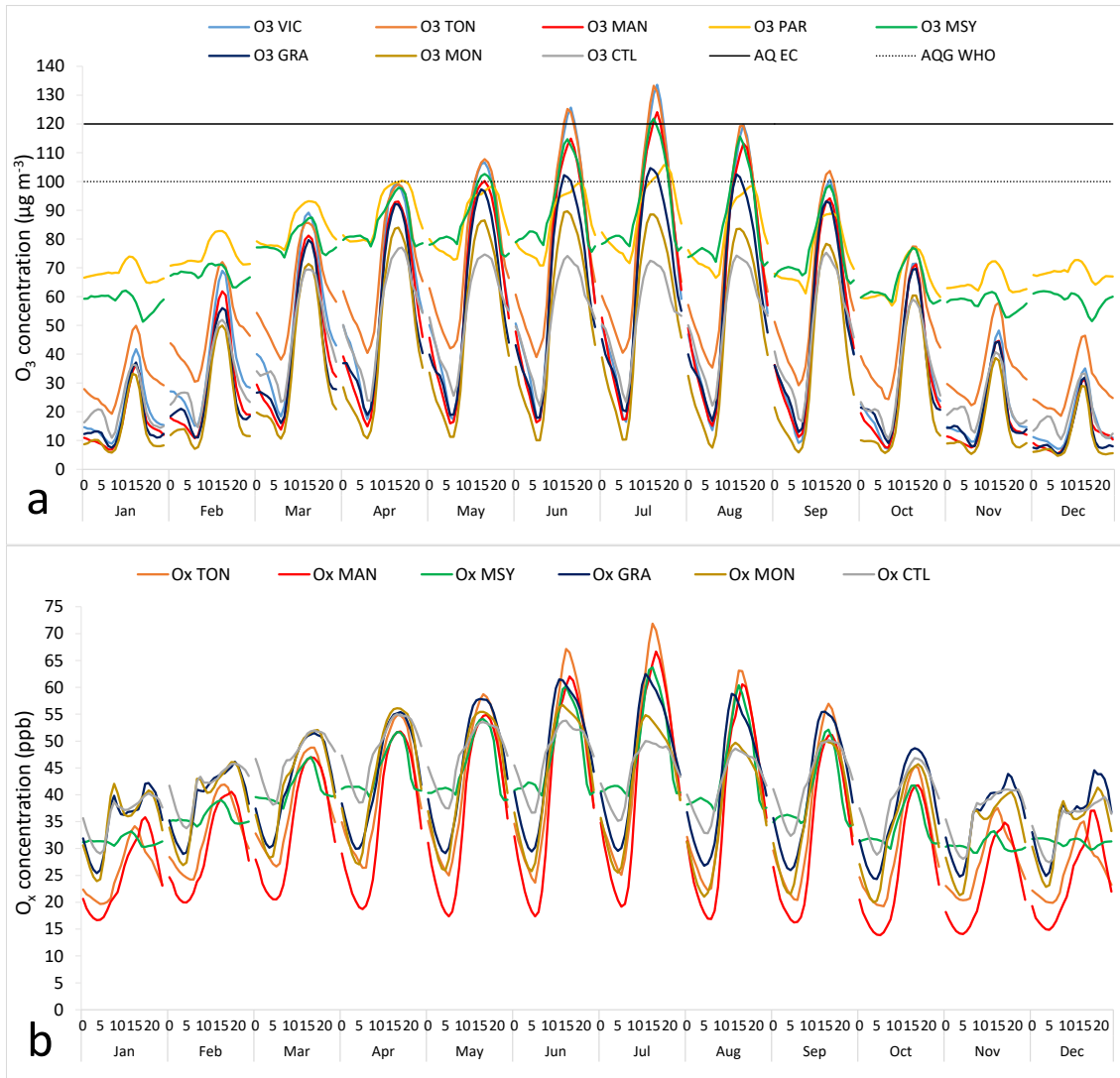


APR-SEP	site	type	period	years	initial concentration	%/year	%/year min	%/year max	%/period	p-Value
NO	CTL	UB	2005-2017	13	9.7	-2.2	-3.7	-1.1	-28.8	*
	MON	SUT	2005-2017	13	20.3	-4.3	-6.2	-3.3	-56.5	***
	MNR	UT	2005-2017	13	11.8	-3.8	-5.9	-1.6	-49.0	**
	VGe	SUT	2005-2017	13	4.8	-4.4	-6.5	-0.4	-57.2	*
NO <sub>2</sub>	CTL	UB	2005-2017	13	42.1	-1.6	-2.8	-0.9	-20.6	***
	MON	SUT	2005-2017	13	36.2	-2.0	-3.0	-1.2	-25.5	**
	MAN	SUB	2006-2017	12	15.7	-1.3	-2.2	-0.4	-15.8	*
	MAT	UB	2006-2017	12	22.2	-1.7	-2.5	-0.4	-19.9	*
	MNR	UT	2005-2017	13	31.0	-1.4	-2.3	-0.4	-18.0	**
O <sub>3</sub>	VGe	SUT	2005-2017	13	19.0	-3.3	-4.3	-2.5	-43.3	**
	ALC	SUI	2005-2017	13	10.3	-1.6	-2.5	0.0	-21.4	+
	CTL	UB	2005-2017	13	45.1	1.4	-0.6	2.4	17.8	+
	MON	SUT	2005-2017	13	41.5	3.2	1.3	6.0	42.1	**
	MAN	SUB	2006-2017	12	58.0	1.3	0.0	2.5	15.9	*
	BdC	RB	2005-2017	13	76.7	-1.6	-2.1	0.0	-20.5	+
O <sub>x</sub>	AGU	RB	2005-2017	13	88.9	-1.1	-1.6	-0.2	-13.8	*
	STP	RB	2005-2017	13	68.7	-1.4	-2.6	-0.8	-18.0	***
	MAT	UB	2006-2017	12	71.6	0.4	-0.3	1.3	4.9	+
	MNR	UT	2005-2017	13	45.6	2.6	1.8	3.5	33.7	***
	ALC	SUI	2005-2017	13	73.9	0.5	0.0	1.5	6.8	**
O <sub>x</sub>	MNR	UT	2005-2017	13	39.1	1.1	0.6	1.5	14.2	***
	VGe	SUT	2005-2017	13	43.1	-0.5	-0.9	0.1	-6.5	+

948 Figure 4



949 Figure 5

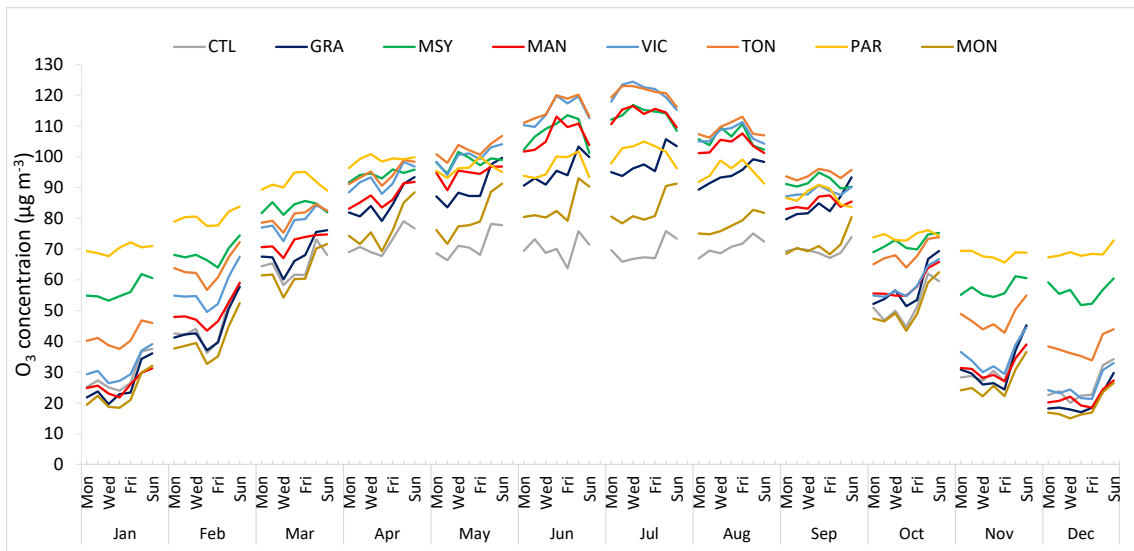


950

951

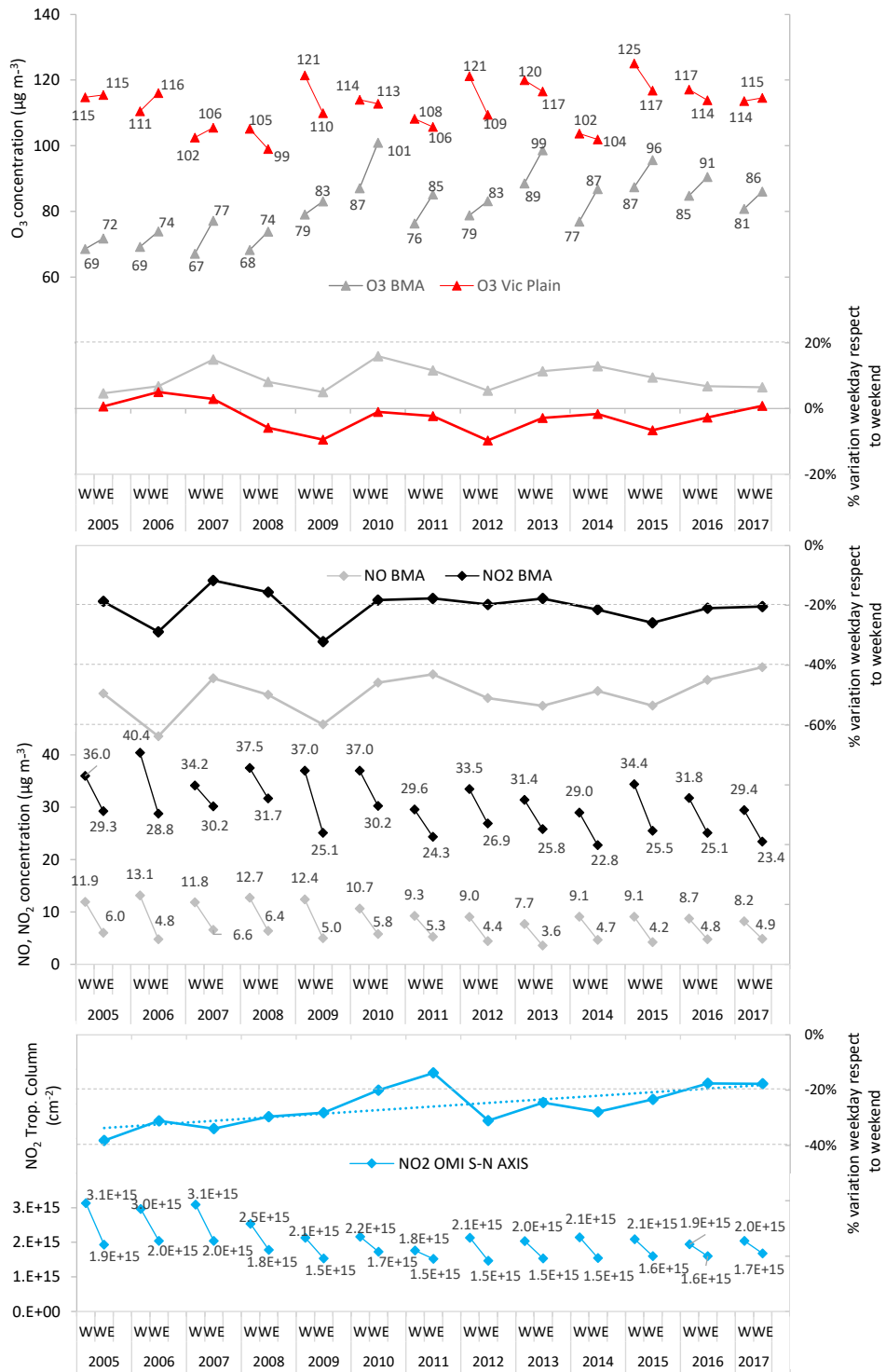
952 Figure 6





953

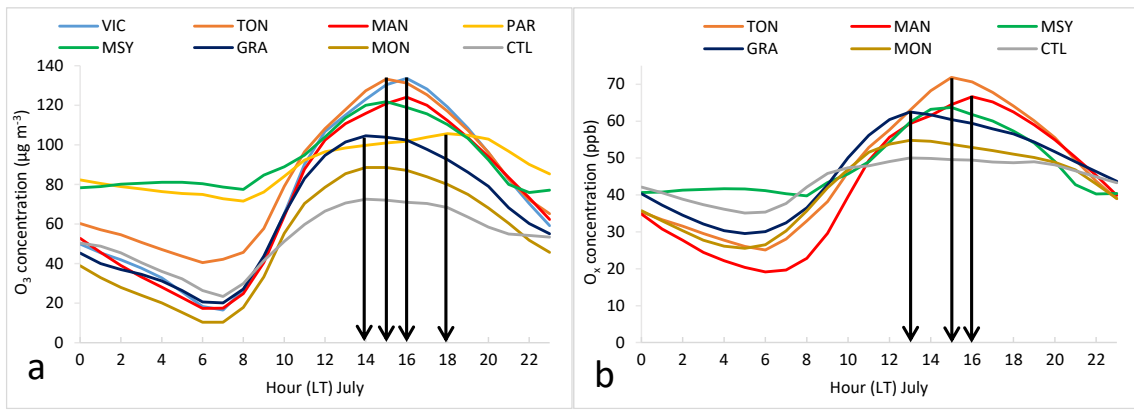
954 Figure 7



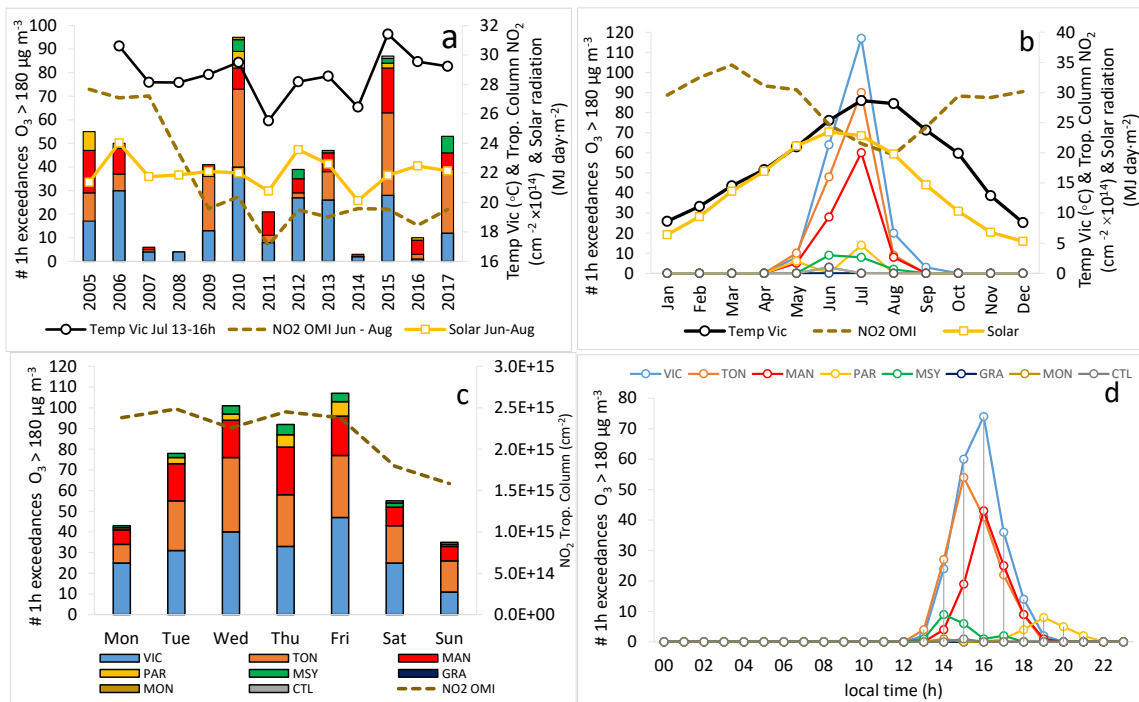
955

956 Figure 8

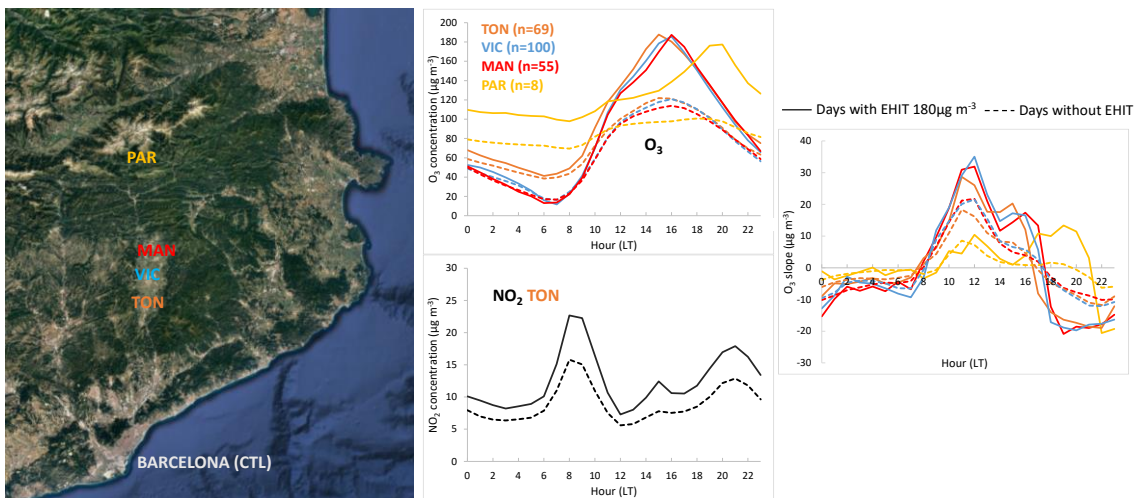
957



958 Figure 9

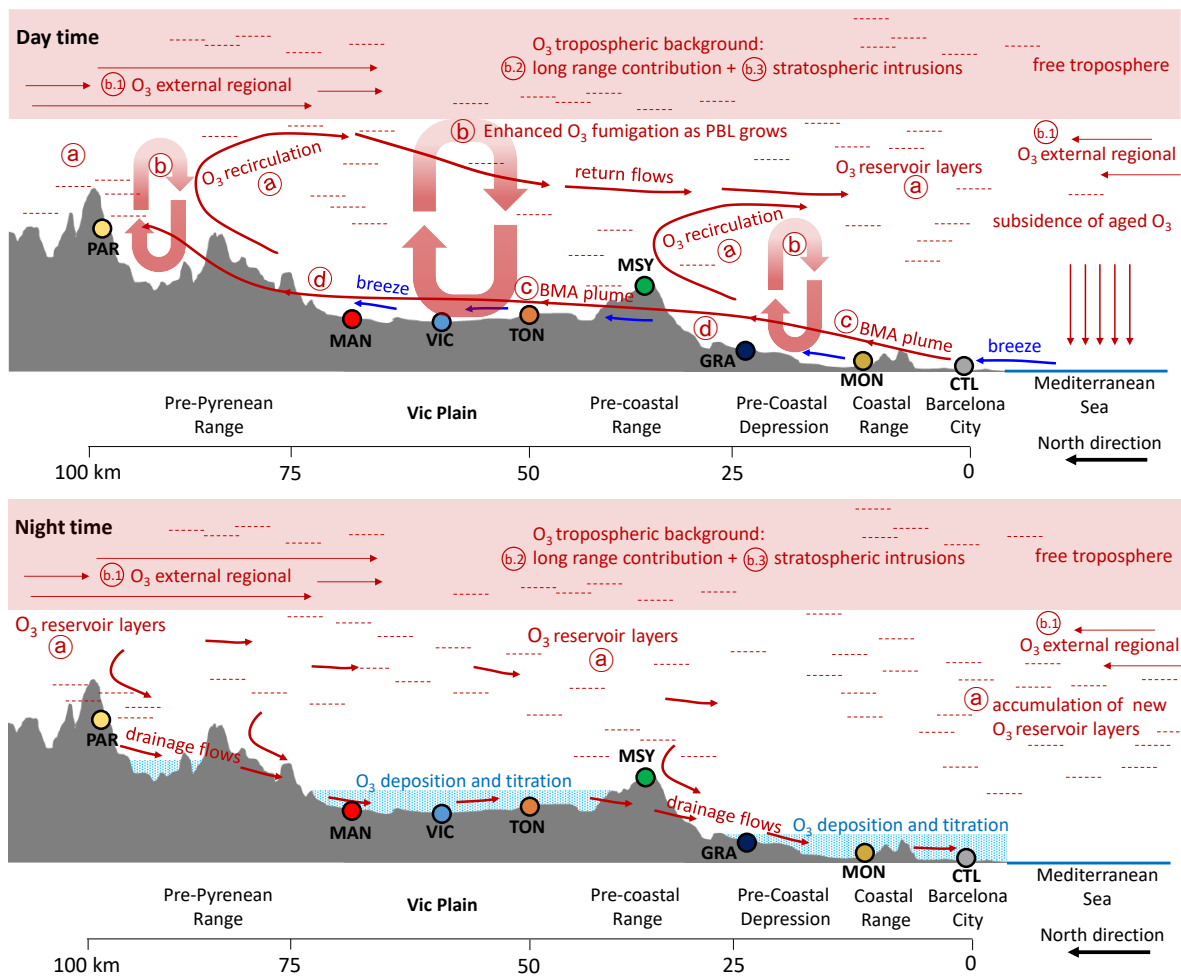


959 Figure 10



960

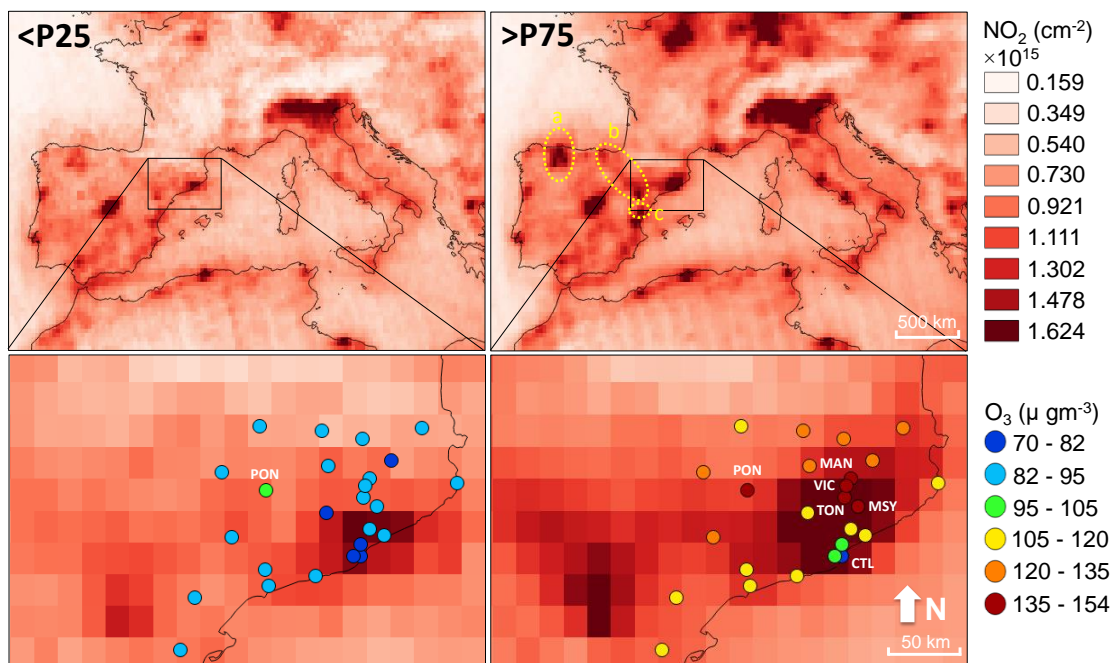
961 Figure 11



962

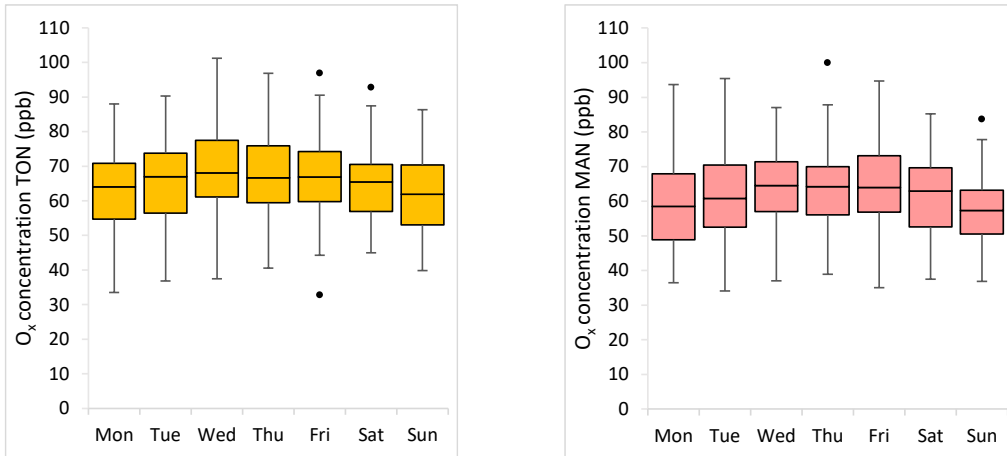
963

964 Figure 12



965

966 Figure 13



Avg. O <sub>x</sub> June & July 12:00 - 19:00 LT (2005-2017)	TON	MAN
maximum percentile 75 (ppb)	77.5 (Wed.)	73.1 (Fri.)
minimum percentile 25 (ppb)	53.0 (Sun.)	48.8 (Mon.)
max. intra week diff: max p.75 - min p.25 (ppb)	24.5 (-32%)	24.3 (-33%)
max average (ppb)	68.0 (Wed.)	64.6 (Wed.)
min average (ppb)	61.5 (Sun.)	56.8 (Sun.)
intra week diff: max avg.- min avg. (ppb)	6.5 (-10%)	7.7 (-12%)

967 Figure 14

968